FEDERAL UNIVERSITY OF PARÁ
INSTITUTE OF GEOSCIENCES
GEOPHYSICS GRADUATE PROGRAM

MASTER DISSERTATION

Petrophysical parameters estimation from well-logs: the shear velocity prediction and density interval inversion cases

MATIAS COSTA DE SOUSA

Belém-Pará

2019

MATIAS COSTA DE SOUSA

Petrophysical parameters estimation from well-logs: the shear velocity prediction and density interval inversion cases

Master Dissertation submitted to the Geophysics Graduate Program of the Geosciences Institute at Federal University of Pará for the obtainment of the title of Master of Science in Geophysics.

Area of study: Petrophysics

Research field: Geophysics applied to the exploration of hydrocarbons

Advisor: José Jadsom Sampaio de Figueiredo

Belém-Pará
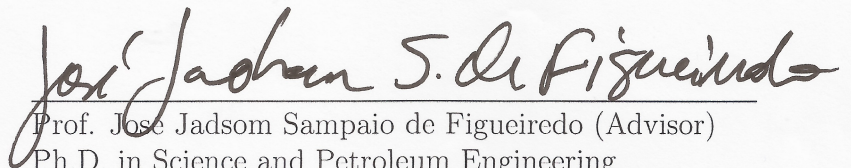
2019

MATIAS COSTA DE SOUSA

Petrophysical parameters estimation from well-logs: the shear velocity prediction and density interval inversion cases

Master Dissertation submitted to the Geophysics Graduate Program of the Geosciences Institute at Federal University of Pará for the obtainment of the title of Master of Science in Geophysics.

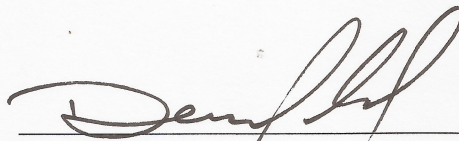Approval Date: March 8, 2019

Grade: EXCELENTE

Committee Members:

Prof. José Jadsom Sampaio de Figueiredo (Advisor)
Ph.D. in Science and Petroleum Engineering
Federal University of Pará

Prof. Paulo Roberto de Carvalho (Member)
Ph.D. in Geophysics
Federal Rural University of Amazônia

Prof. Daniel Leal Macedo (Member)
Ph.D. in Science and Petroleum Engineering
Federal University of Pará

ACKNOWLEDGMENTS

RESUMO

A estimativa de paramêtros petrofísicos a partir de dados de perfilagem de poço é de primordial importância para avaliação da qualidade de reservatórios de hidrocarboneto, tanto para identificação do potencial exploratório, como para controle de poços produtores. Existem propriedades das rochas que são diretamente registradas pelas sondas, como tempo de trânsito de ondas acústicas e densidade da rocha, contudo, informação sobre mineralogia e fração porosa, por exemplo, precisa ser determinada indiretamente. Neste trabalho são desenvolvidos dois estudos sobre parâmetros essenciais para interpretação petrofísica, que são a velocidade da onda S (V_S) e a densidade da rocha (ρ_b). Em conjunto com a velocidade da onda P (V_P), estes parâmetros são úteis principalmente para quantificar módulos elásticos e, consequentemente, verificar propriedades geomecânicas. Além disso, tais parâmetros têm correlação direta com porosidade e litologia das formações atravessadas pelo poço. A primeira parte desta dissertação consiste em um artigo sobre estimativa de V_S a partir de V_P adaptada do método de Greenberg-Castagna, em que se propõe a calibragem de relações empíricas em dados reais. Por sua vez, a segunda parte é um artigo sobre inversão linear intervalar de ρ_b, aplicada também em dados reais, com intuito de obter estimativas das densidades da matriz, dos fluidos e do folhelho na formação. A aplicação das metodologias propostas é realizada em perfis de poços provenientes da plataforma continental da Noruega, em que se verifica a viabilidade de estimar propriedades físicas de rocha que dependem da litogolia local e dos fluidos presentes nas formações geológicas.

Palavras-chaves: Petrofísica. Perfis de poço. Velocidade de onda S. Densidade da rocha. Inversão intervalar.

ABSTRACT

The estimation of petrophysical parameters from well-logging data is of paramount importance to evaluate the quality of hydrocarbon reservoirs, for exploratory potential identification as well as for management of production wells. There are rock properties that are directly recorded by the sondes, such as acoustic waves traveltimes and bulk density, however, information on mineralogy and porous fraction, for instance, requires to be determined indirectly. In this work are developed two studies about essential parameters in petrophysical interpretation, which are the S-wave velocity (V_S) and the bulk density (ρ_b). Coupled with the P-wave velocity (V_P), these parameters are mainly useful to quantify the elastic moduli and, consequently, verify geomechanical properties. Moreover, such parameters have direct correlation to porosity and the lithology of the formations traversed in the wellbore. The first part of this dissertation consists of an article about V_S estimation from V_P adapted from Greenberg-Castagna method, in which is proposed the calibration of empirical relations in real data. In turn, the second part is an article about ρ_b interval linear inversion, also applied in real data, with the purpose of obtaining estimates of matrix, fluid and shale densities in the formations. The application of the proposed methodologies is performed in well-logs from the Norwegian continental shelf, wherein is verified the feasibility of the estimation of rock physical properties that depend on the local lithology and the fluids present in the geological formations.

Keywords: Petrophysics. Well-logs. S-wave velocity. Bulk density. Interval inversion.

LIST OF FIGURES

LIST OF TABLES

CONTENTS

1 INTRODUCTION

Understanding the earth's subsurface is a multidisciplinary challenge that geoscientists are committed to work on. Geophysics uses physical methods (e.g. seismic, gravity, magnetic, electrical and electromagnetic surveys) to provide in-depth information about the rocks and their content, which is a core contribution to overcome this challenge. In hydrocarbon exploration, the well-logging technique is employed to obtain high resolution data about downhole geological formations and, hence, gather local information on petroleum prospects. The quantitative interpretation of these well-logs involves the determination of various petrophysical parameters, which are directly associated to reservoir rock's properties such as porosity, permeability, elastic moduli and bulk density (Avseth et al., 2005).

After the first wireline log was recorded in 1927 by Henri Doll and the Schlumberger brothers, a variety of logging tools have been developed by the petroleum industry to run acoustic, neutron and electrical logs (Ellis and Singer, 2007). Although the overall quality and capability of these logging devices has evolved, there are cost and operation limitations yet to be accounted in the acquisition of petrophysical logs and their derived parameters. Reliable compressional wave velocity (V_p) logs, for instance, are commonly acquired by acoustic devices, however, running proper shear wave velocity (V_s) logs is more expensive and because of that the shear wave information usually is available for a limited number of boreholes drilled in a hydrocarbon field. Currently, the most common approaches to infer V_s data are based on empirical correlations, which is an important method to estimate many other parameters that are difficult to acquire in situ (e.g. shale volume and permeability).

In addition to acoustic wave data, the bulk density (ρ_b) measurements are essential to determine lithology and porosity, thereby composing the group of elastic inputs (V_p, V_s and ρ_b) that plays a central role in hydrocarbon exploration (Vernik, 2016). Traditional quantification of porosity from density or sonic measurements relies on prior lithology identification and assumptions on the individual properties of the bulk fractions (minerals and pore fluids), which may need further estimation if pure lithologies and fluid log response aren't available. Therefore, extracting petrophysical information from well-logs may demand parameter inversion and calibration schemes, otherwise it can led to misinterpretation of reservoir properties.

In this work, we approached two examples of petrophysical parameter estimation that involve integration of well-logs and can be used to refine reservoir analyzes such as amplitude variation with offset (AVO), pore pressure estimation and rock physics modeling (Mavko et al., 2009; Zhang, 2011; Castagna and Backus, 1993). This dissertation is structured in two scientific articles: the first (Chapter 2) evaluates an hybrid modeling for

shear-wave velocity prediction, whereas the second (Chapter 3) presents an interval inversion procedure to estimate mineral and fluid densities. In both articles we work with real datasets of reservoir sandstones from the Norwegian continental shelf. The results achieved in the articles demonstrate the feasibility of the proposed methodologies, which focus on providing valuable information that eventually will feed quantitative interpretation of petrophysical logs (shown schematically in Figure 1.1). Moreover, the dissertation comprises two appendices related to the first article, which describe some features of effective medium theory and fluid substitution analysis.
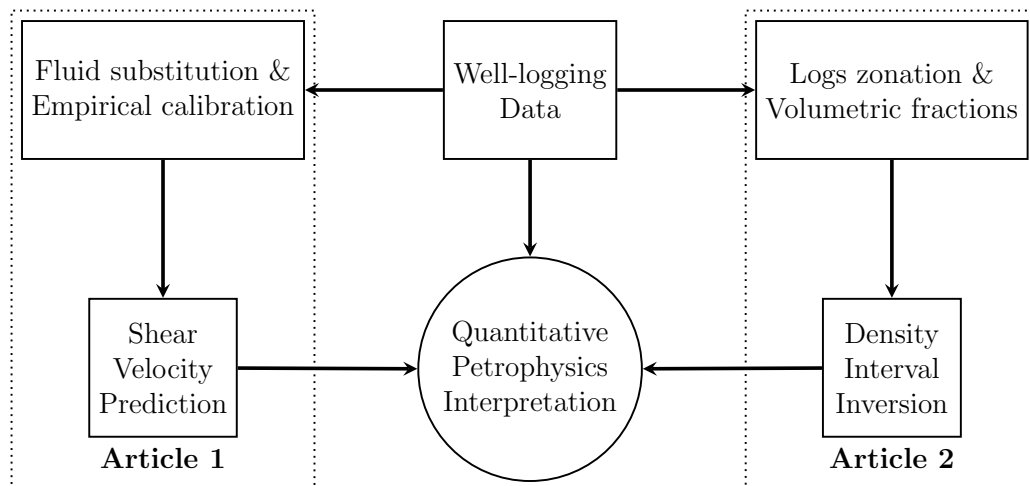
Figure 1.1: Diagram that summarizes the dissertation structure (articles) and its main application (elastic parameters estimation and posterior integration with other well-logs into reservoir evaluation). The S-wave velocity prediction and the inversion of rock density are important to enhance the determination of porosity, permeability, fluid saturations and other elastic-petrophysical quantities based on well-logging data.

2 ARTICLE 1 - PREDICTION OF S-WAVE VELOCITY BY A HYBRID MODEL BASED ON THE GREENBERG-CASTAGNA EQUATION

Matias C. de Sousa, José J. S. de Figueiredo, Carolina B. da Silva, Murillo J. de S. Nascimento

In geophysics, more specifically in rock physics and petrophysics, empirical equations play an important role in data regularization, especially in datasets that are difficult to acquire in situ. In terms of well-logging, a common scenario is the absence of shear wave slowness data, which can be handled by different methods that aim filling data gaps (regularization). This work consists of the application of a hybrid approach (based on Greenberg-Castagna method) to estimate S-wave velocity in brine-saturated lithologies on well-log datasets. The combination of local polynomial regressions with a fluid substitution analysis (Gassmann's equation) leads to an effective method of estimating shear wave velocity (V_S) from compressional wave velocity (V_P) when information about lithology and saturation are available. Well-log datasets (from the Norwegian Sea region) are used to demonstrate the feasibility of our methodology and show its usefulness for dataset regularization based on the local information. We selected learning and test wells from the Norne Field, where Lower to Middle Jurassic sandstones behave as hydrocarbon reservoirs. Our results show that the best fitting between the measured and predicted S-wave velocities were obtained from the modified Greenberg-Castagna method (in this work, named calibrated relation), also verified on a well from the North Viking Graben (validation dataset).

2.1 INTRODUCTION

The quantitative seismic interpretation scope includes several questions related to measurable physical parameters and their interaction on theoretical rock models, which makes a consistent reservoir characterization achievable. Among all elastic modes of propagation, the S-wave mode is the one that has aroused much interest in industry and academia in recent years. Nowadays, S-wave velocities are used frequently when it comes to the characterization of fractured or unconventional hydrocarbon reservoirs (Tokhmchi et al., 2010; De Figueiredo et al., 2012; Santos et al., 2015; Gholami et al., 2016; Biswas and Baruah, 2016). Among all elastic parameters related to rock properties, the shear velocity requires a more rigorous treatment due to the limitations of its recording on

geophysical well-logging or seismic survey, despite the evolution of borehole geophysics' technology (Stevens and Day, 1986; Chen, 1988; Chen, S., 1989; Tang and Wang, 2005; Tan et al., 2015). In this scenario, empirical relations are used to overcome the limitations of S-wave recording.

Shear-wave logging data is often of low quality and, due to acquisition limitations, irregular or even unavailable, mainly in old wells. Historically, restrictions to observe the S-wave arrival on acoustic logs are identified, which implies low reliability of shear slowness measurements on boreholes. For instance, the detection of refracted waves using monopole sources is limited to formations where the S-wave is faster than the drilling mud P-wave. Also, the dispersive nature of flexural waves (dipole sources) and the use of quadrupole sources (LWD) conditioned the acquisitions to low frequencies. Another limitation is observed at formations where the measurements are strongly affected by its anisotropy, especially on directional wells (Cheng, 2015).

A pragmatic alternative to solve the lack of shear velocity information is to use physical-mathematical models that enable its prediction based on more reliable parameters, for example, pure relations between V_P and V_S (Castagna et al., 1985). There are several models developed for this purpose that are very useful for the oil industry (Røgen et al., 2004; Dvorkin and Mavko, 2014). The most famous method is the one developed by Castagna et al. (1985) and improved by Greenberg and Castagna (1992), which uses empirical equations established for specific monomineralic composite and the Biot-Gassmann theory to estimate V_S in brine saturated formations (Gassmann, 1951; Biot, 1956). To ensure that these equations are applied correctly, it is interesting to calculate the regression coefficients using local data, which generally minimizes prediction errors. Based on genetic algorithms and artificial neural networks, Parvizi et al. (2015) developed a cost-effective method for predicting V_S from V_P. Gholami et al. (2014) were able to model S-wave logs using seismic attributes and independent component analysis (ICA). The S-wave velocity prediction is also feasible through intelligent and pattern recognition (by Support Vector Regression-SVR) algorithms (Rezaee et al., 2007; Bagheripour et al., 2015; Nourafkan and Kadkhodaie-Ilkhchi, 2015).

Therefore, V_S log is often predicted using various techniques in order to reduce the logging run cost, but still obtain a representative volume of real data (which is essential to develop alternative approaches for estimating shear velocities). These methods mostly involve rock physics models, heuristic models or empirical models (Han et al., 1986; Krief et al., 1990; Xu and White, 1996; Jorstad et al., 1999; Vernik et al., 2002). Despite being easier to apply, the empirical relations accuracy can't be assured in a single well analysis and usually they are derived for brine-saturated rocks. In contrast, heuristic and rock physics models are robust and have the advantage of being applicable to various types of rocks, however, require input parameters that may be difficult to acquire (information about pore geometry and volumetric fractions of multi-phase complex media). Well-

established prediction models have in common the strong V_S correlation to V_P, density and porosity, which combined to the need of dataset regularization motivates improvements on these methodologies, i.e., increasing the quality of S-wave wireline logging data is a challenge that can be solved by using better quality logs of compressional velocity, density and porosity.

In this work, we propose a modification of the Greenberg-Castagna method to estimate V_S well-logs from V_P logs, considering local information about fluid saturation and lithology. Our proposal is considered a hybrid model in terms of rock physics tools (Avseth et al., 2005). Although our theoretical considerations require more input parameters (water saturation, porosity and clay volume) for its application, our empirical relation is expected to have higher correspondence between local measured P-wave and estimated S-wave velocities. Unlike Greenberg-Castagna, we used the Gassmann fluid substitution theory modified by Mavko et al. (1995) without taking into account S-wave velocity information. Here, we used well-log data (three wells) from the Norne Field to calibrate the empirical equations according to the predominant lithologies of the region, characterized by a sandstone reservoir with intercalated shale formations, in order to compare the efficiency of the calibrated relations with Castagna et al. (1993)'s relations and demonstrate that the adopted methodology is a consistent alternative for predicting shear velocity. In addition, we applied this methodology to a validation dataset (one well) from the North Viking Graben, which is located at the North Sea region (south of Norwegian Sea).

2.2 METHODOLOGY

From the petrophysical point of view, the construction of mathematical models that describe the combination of each rock constituent property is essential, which comes down to volumetrically weigh the composition of the mineralogical matrix and the fluid content of a formation. On the other hand, the simulation of the fluid substitution requires a consistent formulation to be evaluated. At this point we resort to the Biot-Gassmann theory, which is characterized as a tool applicable in well data, limited by the premises discussed in Gassmann (1951) and Biot (1956).

In order to fully understand the methodology applied in this work, we provide a brief description of some important tools of the effective-medium theory that are used to determine the elastic parameters (see Appendix A), which makes the fluid substitution analysis and the application of the Greenberg-Castagna method possible. In addition, we used a least squares fitting approach to calibrate V_P-V_S equations and a P-wave approximation of Gassmann's relation. Therefore, the S-wave hybrid modeling proposed here consists of two main parts that adapt Greenberg-Castagna approach: 1) using a reference dataset to calibrate empirical relations at brine saturated lithologies; and 2) applying P-wave approximation on Gassmann substitution recipe to predict V_S any saturation.

2.2.1 Greenberg-Castagna method

To estimate the S-wave velocity (V_S) from other petrophysical parameters, Greenberg and Castagna (1992) presented a mathematical model based on linear relations of V_P, applied on brine-saturated multimineralic rocks. They used the coefficients presented in Table 2.1, which satisfy the expression

$$V_S = \frac{1}{2}\left\{ \left[\sum_{i=1}^{L} f_i \sum_{j=0}^{N_i} a_{ij} V_P^j \right] + \left[\sum_{i=1}^{L} f_i \left(\sum_{j=0}^{N_i} a_{ij} V_P^j \right)^{-1} \right]^{-1} \right\}, \tag{2.1}$$

where L is the number of monomineralic components, f_i is the volumetric fraction of the i-th component, a_{ij} are the coefficients of the empirical regression, N_i is the degree of the polynomial for i-th lithology constituent (mineral and fluids), V_P^j and V_S are the compressional and the shear velocities (in km/s), respectively. Greenberg-Castagna equation approximates the shear-wave velocity by a simple average of the arithmetic and harmonic means of the constituent pure-lithology shear velocities, i.e., V_P is used to estimate $V_S = a_{i2} V_P^2 + a_{i1} V_P + a_{i0}$ for each single lithology and then the composite effective V_S is obtained (Avseth et al., 2005).

Obtained by Castagna et al. (1993), the empirical coefficients in Table 2.1 were calculated for 100% brine saturation and, for this reason, to estimate V_S in the *in situ* condition it is necessary to apply fluid substitution calculations. The original procedure of the method involves performing several iterations starting from assumptions of V_P for brine until reaching a significant convergence, thus ensuring the quality of the V_S estimation. The hybrid approach in question relies on an approximation of the relation (B–3) (see Appendix B) to obtain the shear velocity from the compressional velocity, avoiding the iterative processes.

Table 2.1: Regression coefficients of V_S presented by Castagna et al. (1993)

Lithology	a_{i2}	a_{i1}	a_{i0}	R^2
Sandstone	0	0.80416	-0.85588	0.98352
Limestone	-0.05508	1.01677	-1.03049	0.99096
Dolomite	0	0.58321	-0.07775	0.87444
Shale	0	0.76969	-0.86735	0.97939

2.2.2 Petrophysical and elastic parameters obtained from well-log data

As well as elastic parameters, petrophysical ones play an important role on the application of effective-medium models. There are some methods of extracting this information from well-logs and, using complementary data (core analysis), it is possible to compute accurate fractions of all rock constituents, but the use of wireline logs in isolation imply

limited models. The conventional approach is to consider clay and a second constituent (e.g. quartz for sandstone) on the matrix, as well as water and other fluid on the pores. Taking into account that the clay content controls the radioactive response of geologic formations, the fractions of the lithologic (mineral) components can be obtained based on the gamma-ray log, using the equations

$$I_{GR} = \frac{GR - GR_{min}}{GR_{max} - GR_{min}}, \tag{2.2}$$

$$v_{shale} = 0.33(2^{(2I_{GR})} - 1), \tag{2.3}$$

and

$$v_{sand} = 1 - v_{shale}, \tag{2.4}$$

where GR_{max} and GR_{min} are the maximum and minimum values evaluated from the gamma-ray log (GR), v_{shale} and v_{sand} denote content of shale and fraction of sandstone, respectively. Throughout the formations traversed in each well, the I_{GR} (radioactivity index) is calculated and then applied in the relation of Larionov (1969) (equation (3.5)), which is coherent for old rocks..

Both velocities (in km/s) are evaluated from sonic slowness logs (in $\mu s/ft$), whose conversion is performed according to the equation (2.5), as another important petrophysical parameter, the total porosity (ϕ), that can be estimated from the compressional slowness (Δt_p):

$$V = \frac{304.8}{\Delta t}, \tag{2.5}$$

and

$$\phi = \frac{\Delta t_p - \Delta t_{min}}{\Delta t_{fl} - \Delta t_{min}}, \tag{2.6}$$

wherein Δt_{min} and Δt_{fl} are the traveltimes of the P-wave for mineral and fluid phases, respectively. The constants $(\Delta t_p, \rho)$ used to compute all these parameters are shown in Table 2.2, as well as the elastic moduli (K,μ) to be considered in the V_S estimation.

Table 2.2: P-wave slowness (Δt_p), density (ρ), bulk modulus (K) and shear modulus (μ) of minerals and fluids used for modeling the rock effective properties (Mavko et al., 2009). (1): in $\mu s/ft$. (2): in g/cm^3. (3): in GPa.

Component	$\Delta t_p^{(1)}$	$\rho^{(2)}$	$K^{(3)}$	$\mu^{(3)}$
Quartz	55	2.65	37	44
Clay minerals	89	2.58	21	7
Brine	185	1,1	3.2	0
Water	189	1	2.2	0
Oil	230	0.85	0.8	0
Gas	920	0.2	0.02	0

2.2.3 Velocities' polynomial regression

An essential part of this work is the determination of polynomial regression coefficients that best fit the velocities for the (local) lithology analyzed here. In order to obtain a model that can predict the shear velocity with greater accuracy, we use least squares analysis, which consists of adjusting the S-wave to P-wave velocity logs adopting a linear model described by a polynomial function. This method of curve fitting allows us to obtain the coefficients of the polynomial (2.7) that best correlates V_S to V_P (minimum error ϵ), which is represented in matrix terms by equation (2.8):

$$V_S = a_n V_P^n + a_{n-1} V_P^{n-1} + \ldots + a_1 V_P + a_0 + \epsilon, \tag{2.7}$$

$$\begin{bmatrix} a_0 \\ a_1 \\ \vdots \\ a_n \end{bmatrix} = (\boldsymbol{X}^T \boldsymbol{X})^{-1} \boldsymbol{X}^T \begin{bmatrix} V_{s1} \\ V_{s2} \\ \vdots \\ V_{sm} \end{bmatrix}, \tag{2.8}$$

where

$$\boldsymbol{X} = \begin{bmatrix} 1 & V_{p1} & \cdots & V_{p1}^n \\ 1 & V_{p2} & \cdots & V_{p2}^n \\ \vdots & \vdots & \ddots & \vdots \\ 1 & V_{pm} & \cdots & V_{pm}^n \end{bmatrix}, \tag{2.9}$$

and each velocity log (V_P and V_S) contains m elements in depth. Based on v_{sand} and v_{shale} the velocity logs of a given well are divided into two sets: one corresponding to the clean formations and the other to the shaly formations. In these partitioned logs one can apply this method of polynomial regression and thus calibrate the empirical relationships for sandstones and shales. Although the maximum polynomial order is given by $m-1$, in practice we use an arbitrary order as low as possible to accurately describe the dataset.

2.2.4 P-wave approximation of Gassmann's relation

To estimate the changes in acoustic velocities, when pore content is altered, it is necessary to know both velocities on an initial saturation condition in order to apply the Gassmann's transformation based on the bulk moduli of the rock and its components (matrix and fluids). In the scenario in which only the V_P log is regular, it becomes feasible to use the P-wave modulus (M) based on the equations

$$M = \rho_b V_p^2 = K + \frac{4}{3}\mu, \tag{2.10}$$

and

$$\frac{M_{sat}}{M_{min} - M_{sat}} = \frac{M_{dry}}{M_{min} - M_{dry}} + \frac{M_{fl}}{\phi(M_{min} - M_{fl})}, \tag{2.11}$$

where the subscripts *sat*, *dry*, *min* and *fl* indicate saturated rock, dry rock, mineral matrix and fluid, respectively. Also called longitudinal modulus, M expresses the compressive strength in a state of uniaxial stress (direction of propagation of the P-wave). All the elastic moduli are given in GPa here.

According to Mavko et al. (1995), the approximate transformation (2.11) makes it possible to achieve results similar to the original transformation (B–3). By means of this relation it is possible to use a straightforward application of the weighted average of the empirical relations of V_P-V_S (Greenberg-Castagna equation) in the condition of brine saturation (without requiring a convergence analysis), reducing V_S prediction cost without significant quality losses. Starting from a given *in situ* condition, denoted by index (1), the fluid replacement recipe to be applied for the purpose of estimating V_s (using local empirical relations) in a saturated brine condition, denoted by index (2), consists of:

1. Extract the P-wave modulus in the initial condition:

$$M_{sat}^{(1)} = \rho_b^{(1)} \left(V_P^{(1)} \right)^2;$$

2. Use the approximate Gassmann's transformation to calculate the new P-wave modulus:

$$M_{sat}^{(2)} = \frac{x}{(1+x)} M_{min}$$

$$x \equiv \frac{M_{sat}^{(1)}}{M_{min} - M_{sat}^{(1)}} - \frac{M_{fl}^{(1)}}{\phi(M_{min} - M_{fl}^{(1)})} + \frac{M_{fl}^{(2)}}{\phi(M_{min} - M_{fl}^{(2)})};$$

3. Calculate the new density: $\rho_b^{(2)} = \rho_b^{(1)} + \phi(\rho_{fl}^{(2)} - \rho_{fl}^{(1)})$;

4. Obtain the P-wave velocity for brine saturation:

$$V_P^{(2)} = \sqrt{\frac{M_{sat}^{(2)}}{\rho_b^{(2)}}};$$

5. Estimate the velocity of the S-wave for brine saturated formation using the local empirical relations and, finally, obtain it for the *in situ* condition:

$$\mu_{sat}^{(1)} = \mu_{sat}^{(2)} = \rho_b^{(2)} \left(V_S^{(2)} \right)^2,$$

and

$$V_S^{(1)} = \sqrt{\frac{\mu_{sat}^{(1)}}{\rho_b^{(1)}}} = V_S^{(2)} \sqrt{\frac{\rho_b^{(2)}}{\rho_b^{(1)}}}.$$

This procedure highlights the theoretical side of the proposed model, which, when taking into account the approximation of Gassmann's relation for P-wave modulus, becomes

simpler than the methodology proposed by Greenberg and Castagna (1992). Figure 2.1 shows a flowchart summarizing the methodology developed in this work.
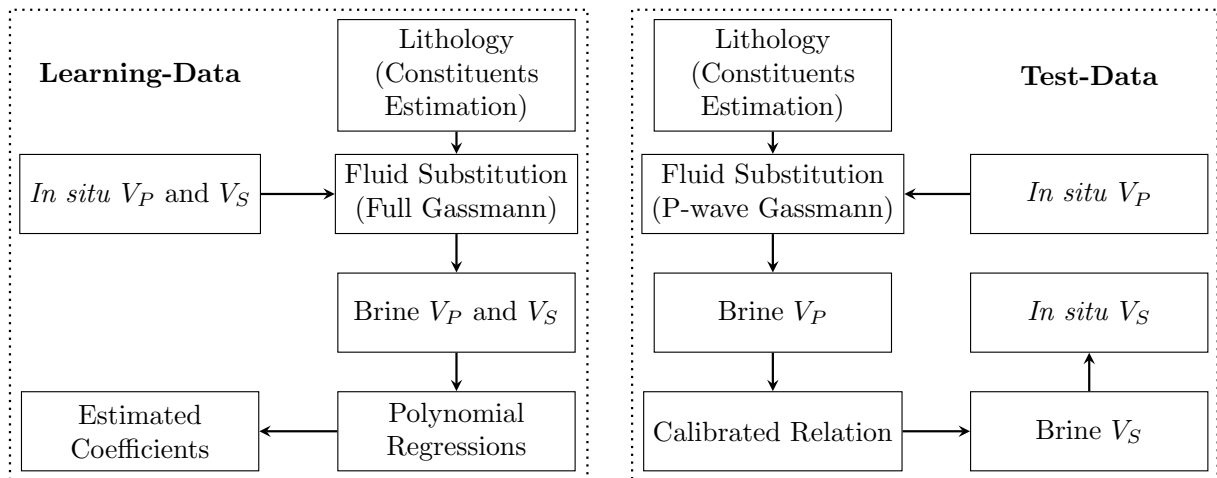
Figure 2.1: Modeling flowchart. First, the empirical relationships are calibrated using the learning-data from a reference well (left branch): the model is calibrated starting with V_P, V_S and the rock constituents (mineral fractions, fluid saturations, porosity and density). Then, they are tested on other wells to predict the *in situ* shear velocity (right branch).

2.3 RESULTS AND DISCUSSION

The two sets of well-log data analyzed in this work were from the North Sea region. The first was from the Norne Field and the second from the Viking Graben field. These two fields are located at the Norwegian continental shelf. Related to the Norne field, Figure 2.2 shows a map illustration of the Norne location. This picture is modified from Gjerstad et al. (1995), which has a geological description of this oil field. Figure 2.3 shows that the Viking Graben is a nort-south-trending linear trough straddling the boundary between the Norwegian and UK sectors of the northern North Sea. This Figure is modified from Brown (1991) and Glennie and Underhill (1998). In these two last literatures, it can be found a detailed description about the geologic features of the Viking Graben area.

The available dataset from the Norne field contains geophysical logs of several wells operated by the Norwegian oil company Statoil ASA, since the beginning of the exploration at the Norne Field, which is located in the Norwegian Sea. Three of these were selected to evaluate the proposed shear velocity prediction model, which we called Well A, Well B and Well C (as shown in Figure 2.4). The inputs for the calibration process and the prediction tests can be divided in: petrophysical parameters (porosity, shale volume and water saturation), which are used to quantify lithology and fluid content; and elastic parameters (bulk density, P- and S-wave velocities), which are the main elements for fluid substitution. The depths of fluid interfaces identified on these boreholes are shown on Table 2.3 and displayed over the logs in Figure 2.5. Hydrocarbons affect the porosity logs making neutronic porosity readings inferior to the estimated density porosities, which is

more noticeable on the shallow thin region of Well B where the difference between the porosities is larger due to gas presence. Furthermore, the Norne Field reservoir rocks consist of interbedded Lower-to-Middle Jurassic sandstones and shales (Statoil, 2001), which we consider the two constituents (quartz and clay) to be evaluated from the gamma-ray readings.
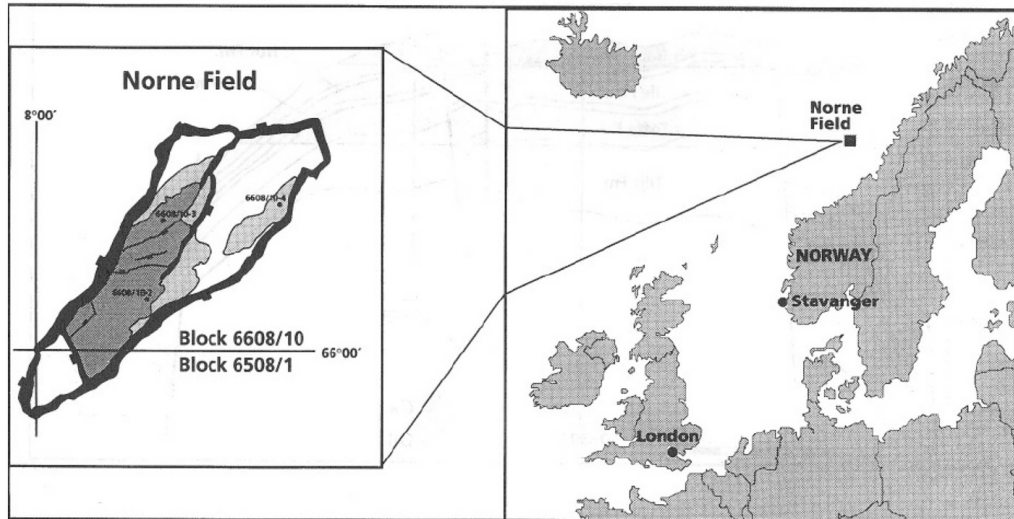
Figure 2.2: The Norne Field in an area of Norwegian continental shelf. This oil field is located in the blocks 6608/10 and 6508/1 in Nordland II. This picture is modified from Gjerstad et al. (1995).
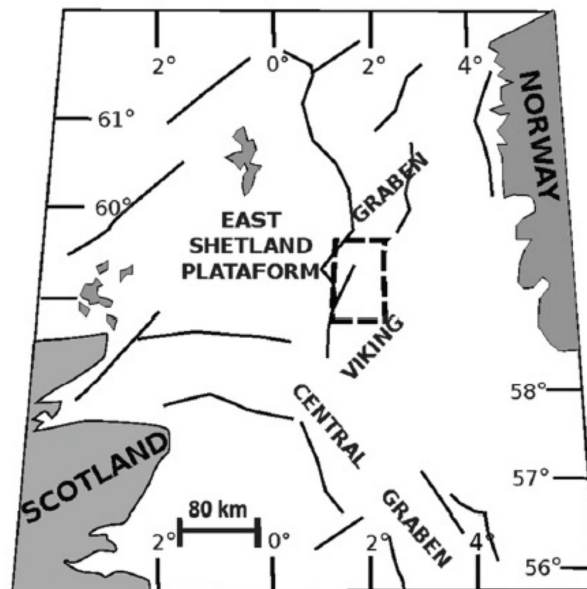
Figure 2.3: The black rectangle shows the area of the Viking Graben oil field. This Viking Graben map was modified from Brown (1991) and Glennie and Underhill (1998).

Table 2.3: Order of the fluid contacts along the investigated wells (in m) (Statoil, 2001). GOC: Gas-Oil Contact. OWC: Oil-Water Contact.

Interface	Well A	Well B	Well C
Reservoir Top	2849.0	3348.0	2706.5
GOC	absent	3361.5	absent
OWC	absent	3487.0	2808.0
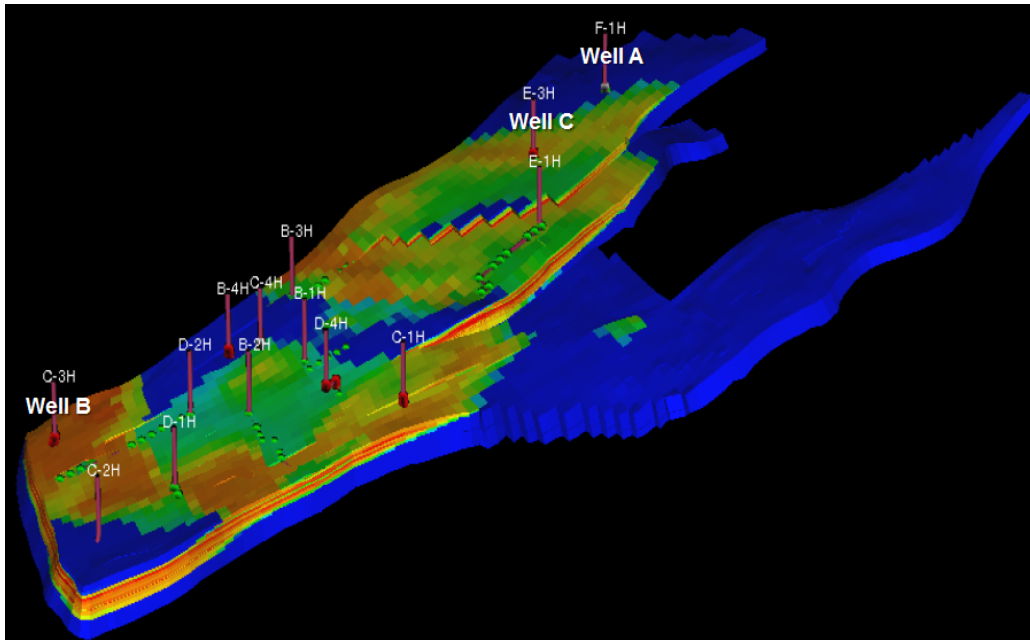
Figure 2.4: Depictional 3D model of the Norne Field with well locations (adapted from Yasin (2012)). Well A (F-1H) is the learning data. The test data is from Well B (C-3H) and Well C (E-3H).

2.3.1 Calibrated empirical relations

Well A presents the porous fraction predominantly filled by water (see Figure 2.5a) along its entire depth interval and, for this reason, it was adopted as a reference-well to calibrate the empirical relationships for sandstone and shale of the Norne Field formations. In order to apply the polynomial regressions in the reference-well, it was necessary to estimate the sonic velocities in the 100% brine condition. Only for this well, the P-wave modulus transformation wasn't applied, since the goal was to obtain the best possible adjustment and then to test it on the other two wells.

In this step, the Voigt-Reuss-Hill relations (Voigt, 1910; Reuss, 1929; Hill, 1963) (equations A–1, A–2 and their average) were used to calculate the density and the bulk modulus of the fluid, taking into account the water saturation to define the volumetric fractions of the formation fluids, and also to estimate the modulus of the matrix, considering the fractions of quartz and clay. In order to determine if the saturated rock bulk modulus was consistent with the fluid saturation of this reference-well, the Hashin-Shtrikman limits

were applied (equation A–3). It was possible to note that the elastic bounds were satisfied both before and after the fluid exchange simulation (see Figure 2.6a and 2.6d). At first, *quartz* is assumed to be the stiffest component of the formation and *water* as the softest constituent, and then the pore content is replaced by *brine*.
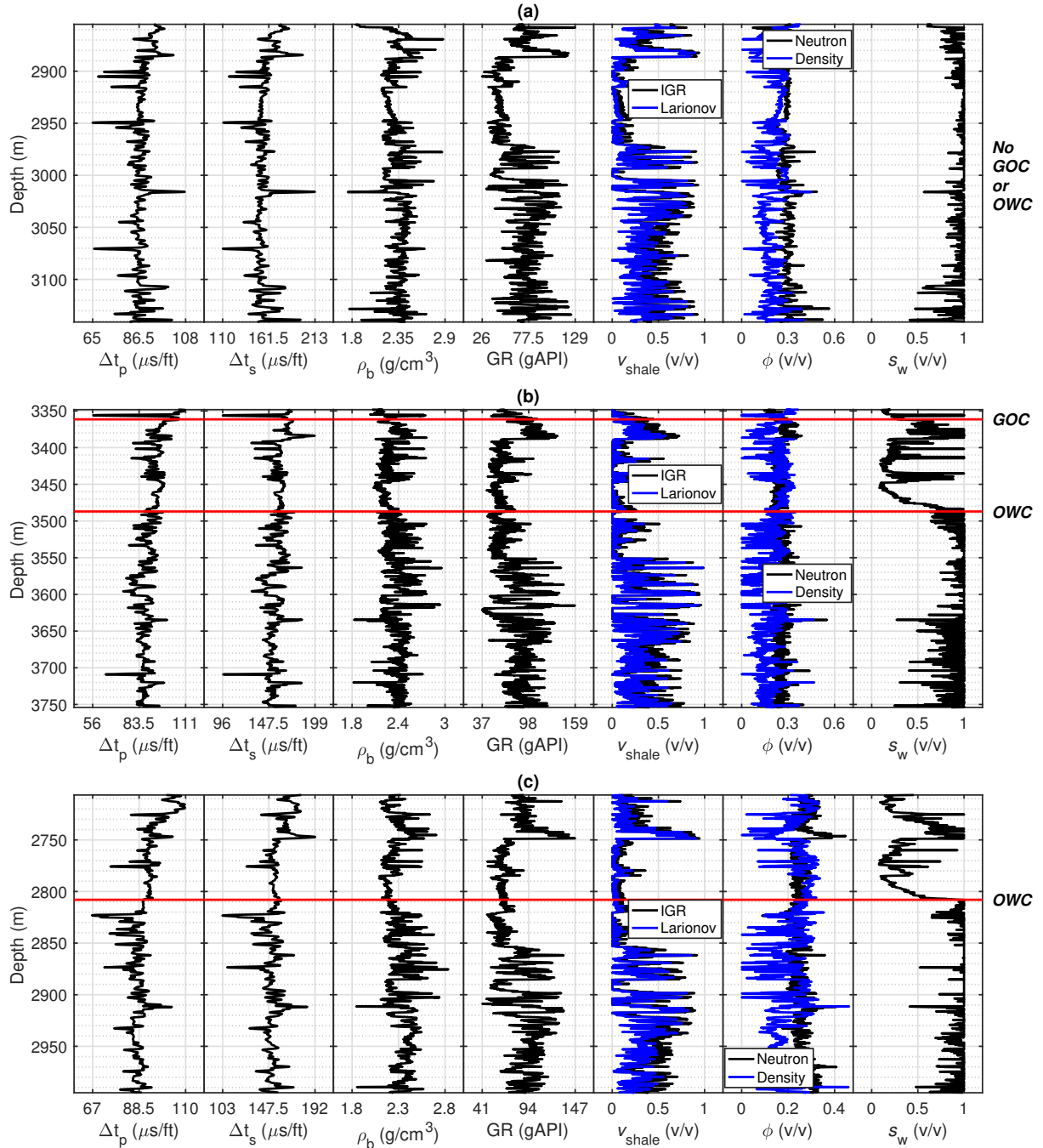
Figure 2.5: Logs of (a) Well A, (b) Well B and (c) Well C. The following parameters for each log are: (from left to right) P-wave traveltime (Δt_P), S-wave traveltime (Δt_s), bulk density (ρ_b), gamma ray GR, shale volume (v_{shale}), porosity (ϕ) and water saturation (s_w).
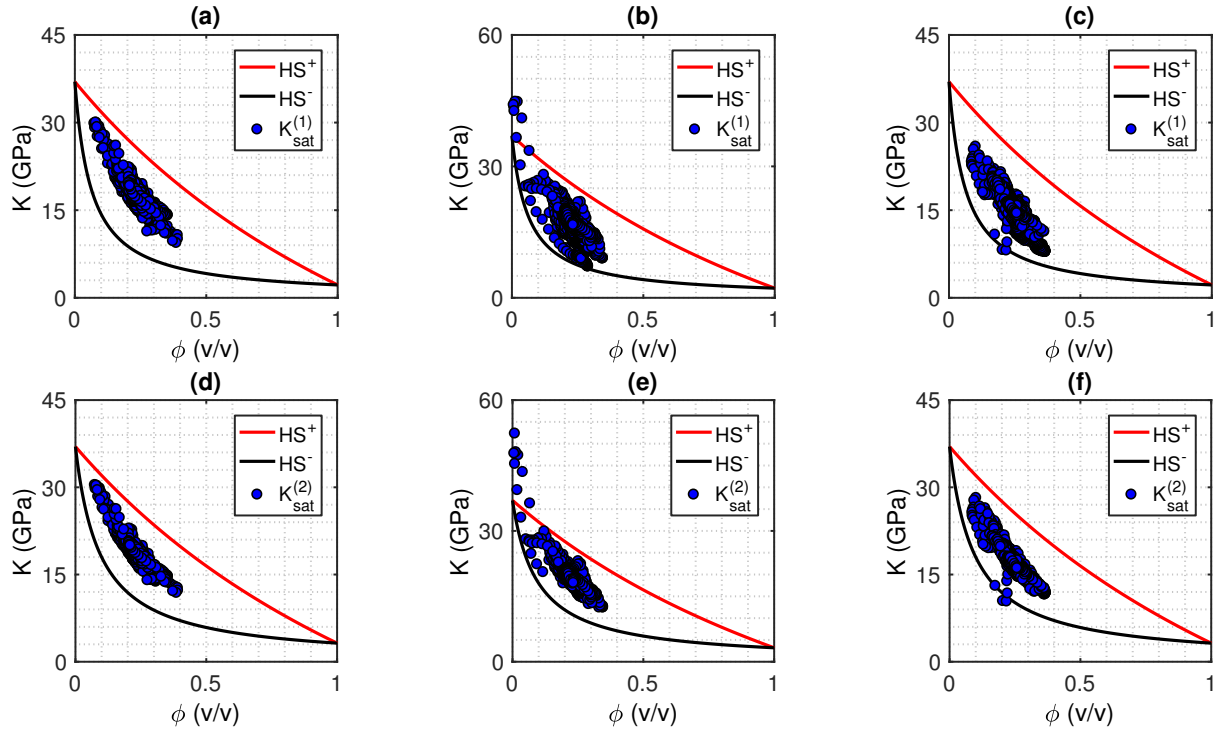
Figure 2.6: Effective bulk modulus of wells A (a,d), B (b,e) and C (c,f). In the top (a,b,c) are the bulk modulus with initial *in situ* saturation and in the below (d, e, f) are the bulk modulus correspondent to brine saturation.
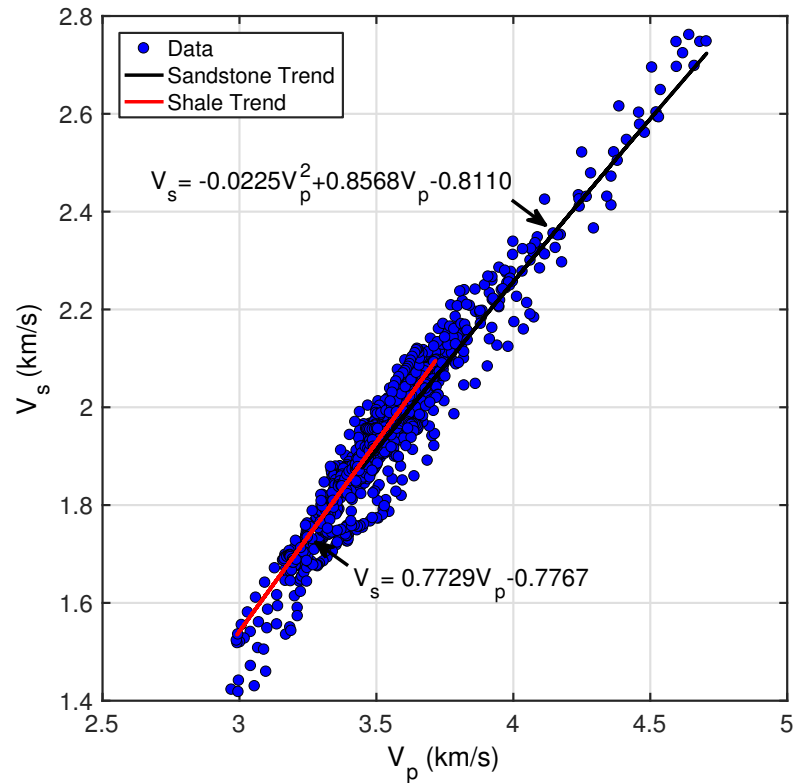
Figure 2.7: Trend curves observed on the Well A velocities for brine saturation. The coefficients of determination are $R^2 = 0.977 = 97.7\%$ and $R^2 = 0.986 = 98.6\%$ for shale line and sandstone parabola, respectively.

Figure 2.7 shows the results of the calibration: a parabola for sandstones and a straight line for shales. As expected, a smaller deviation between measured and estimated velocities obtained by the local (calibrated) relation is observed when compared to the deviation obtained using the original Greenberg-Castagna relation (see Figures 2.8 and 2.9). The high coefficients of determination (R^2) reflect this good fitting, as observed in the regressions with the velocity sets of each lithology (which were selected according to clay and quartz fractions in the rock matrix).

It was also verified the coherence of the S-wave velocity data in relation to the lithologies, since the more shaly the formation, the lower the velocity is (due to the lower elastic modulus of shales in comparison to clean sandstones). For sandstone layers the largest observed variation of V_S is between 1.76 and 3.17 km/s, while for shales the longest variation is between 1.52 to 2.37 km/s.

2.3.2 Shear velocity predictions

Based on the local relations shown in the Figure 2.7, the last stage of this work was performed. We verified the quality of these equations when applied together with the fluid substitution (using approximation (2.11)), i.e., to analyze how reliable it is to predict V_S from V_P with this hybrid model. For the test wells, M_{min}, M_{fl} and ρ_{fl} were calculated using the elastic bounds in a manner similar to the calibration step: obtaining M_{sat} in the brine saturation condition after applying the fluid substitution recipe and calculating V_S by means of the elastic moduli definitions. In order to verify the physical consistency of the elastic properties for the initial and final saturation situations, we used the limits defined by Hashin-Shtrikman.

The bulk modulus distribution on Well B shows values over the upper limit of *quartz-water* and the *quartz-brine* mixtures (see Figure 2.6b and 2.6e), which can be related to calcite cements that are stiffer than quartz (Castagna et al., 1985), but the majority of the values estimated for the two saturation conditions are scattered within the delimited region by the curves HS^+ and HS^-. We also noticed that here the substitution of gas for brine leads to more significant changes in the bulk modulus than in wells A and C, where no oil-gas contact is observed. In the case of Well C, the results were even more satisfactory, showing a good behavior of K_{sat} for the formations in which the fluid substitution (oil, water or gas) by brine was simulated. Samples that are above the upper limit may be associated with formations where calcareous or carbonate content dominates in relation to quartz, which is softer than the minerals calcite and dolomite (see Figure 2.6c and 2.6f). For bulk modulus values near or below the lower limit, either the hydrocarbons predominate in the fluid phase of the formation or the presence of softer clays in the matrix is more expressive.

For comparative purposes, we chose to estimate the shear velocity logs with both the empirical equations of Castagna et al. (1993) and the calibrated relation. The predictions are shown in velocity logs (in blue or red) overlaid by the measured velocity (in black) in Figure 2.8, and then presented in scattering diagrams of estimated versus measured velocity in Figure 2.9. It is observed that the prediction of V_S is reasonable in both cases, with the highest accuracy being observed when applying the local relation (calibrated relation), except for the Well C, wherein the local relation error was slightly greater than the Greenberg-Castagna estimation error for some intervals.
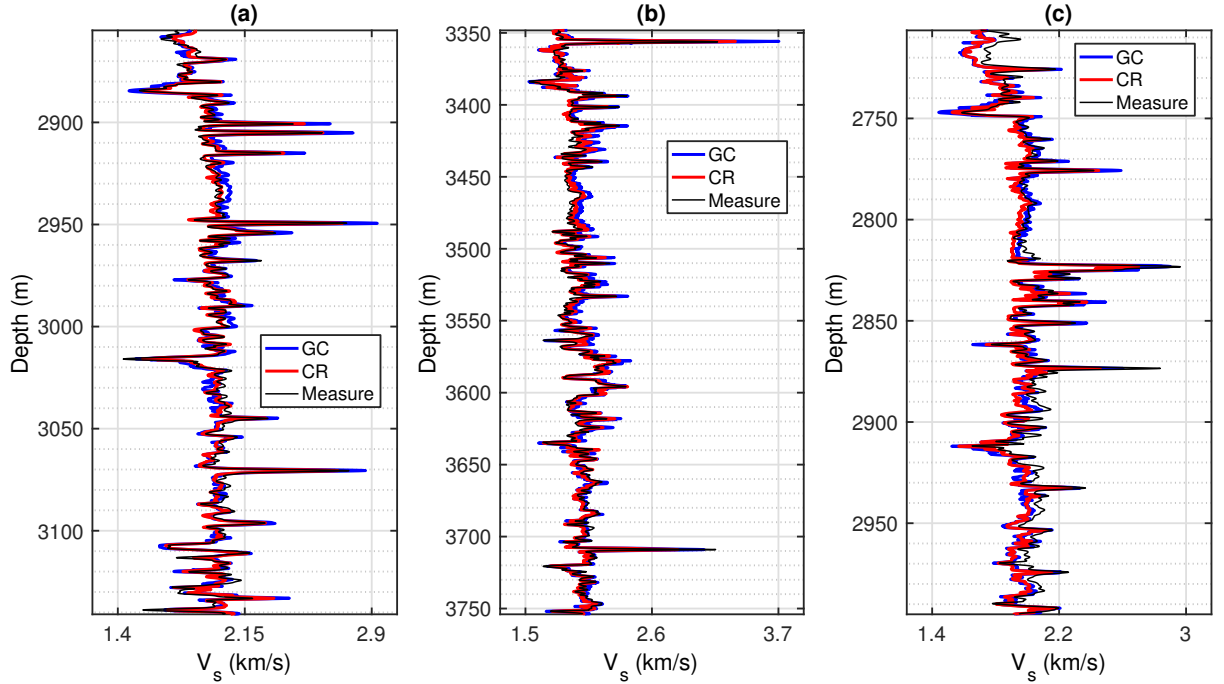
Figure 2.8: Comparisons between V_S logs (measured) with logs predicted using Greenberg-Castagna (GC) and the calibrated relation (CR) for (a) Well A, (b) Well B and (c) Well C. Here, the calibrated relation is our modification of Greenberg-Castagna equation.
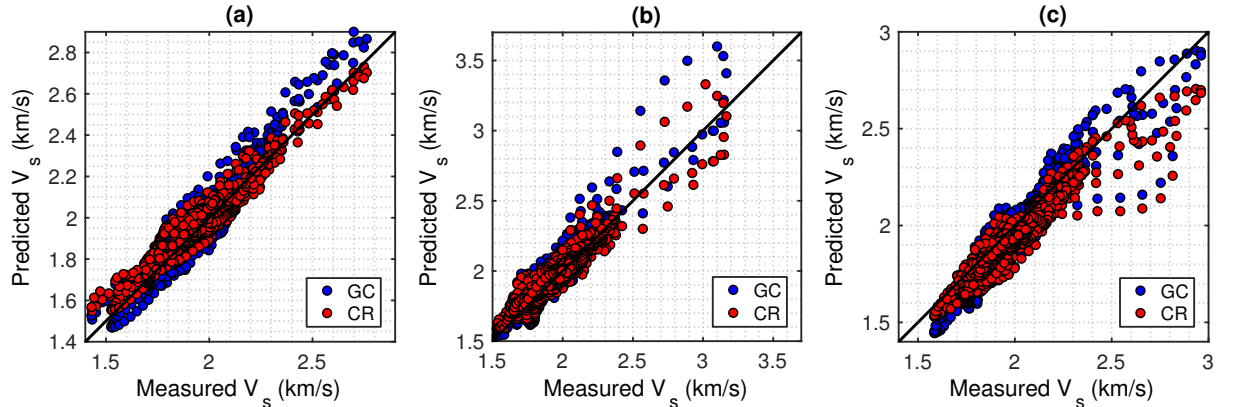
Figure 2.9: The same comparisons performed in the Figure 2.8 using the correlation graph between V_S scatter points (measured) with scatter points predicted using Greenberg-Castagna (GC) and the calibrated relation (CR) for (a) Well A, (b) Well B and (c) Well C.

In general, for well C, despite presenting abrupt deviations (in the depth intervals of 2715-2735 m and 2920-2985 m), the difference between estimated and measured values is considerably small, leading to high prediction quality. The abrupt deviations can be related to irregular velocity measurements due to formation fractures. According to Fertl and Rieke (1980), in case of reservoirs located in regions where there is a strong presence of fractures, e.g. Norne Field, the occurrence of these variations is expected. This effect can also be noted on gamma ray logs, which in the investigated wells present intervals of great instability. On the V_S log of Well B, one large spike (3360 m) and another of median amplitude (3710 m) are noted, which contain the velocities that reach (or exceed) 2.5 km/s. Also, the highest V_S values on Well C are near two median spikes (2825 and 2875 m), indicating that the correlation between the measured and predicted shear velocities loses quality due to this anomalous sonic measurements.
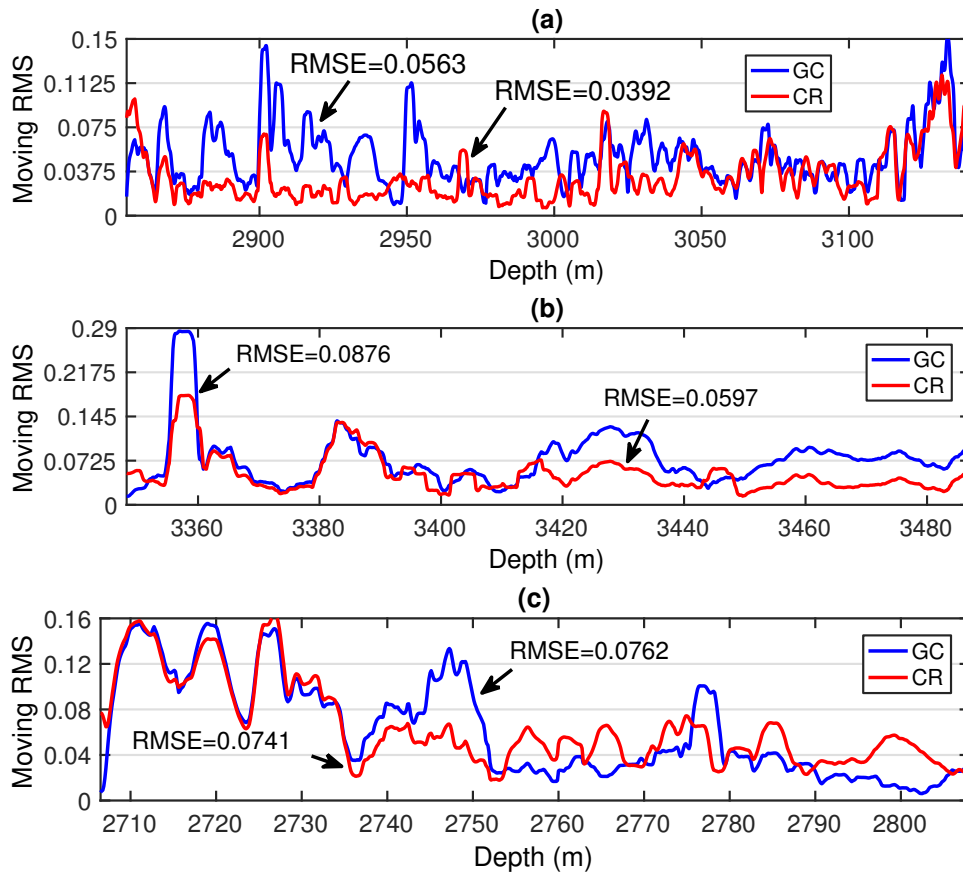
Figure 2.10: The RMSE values for wells (a) A, (b) B and (c) C. The curves in blue color (GC: Greenberg-Castagna) and red color (CR: Calibrated Relations) shows the error between the predicted and measured V_S logs.

In quantitative terms, the *Root Mean Squared Error* (*RMSE*) was evaluated for all wells. Figure 2.10 shows the RMSE logs, i.e., the difference in results between the conventional Greenberg-Castagna method and the calibrated relation. As expected, the RMSE logs for the reference-well, using the calibrated relation, presented values smaller than the RMSE of the other wells and than the RMSE associated to the Greenberg-Castagna

equation. For the other two wells in which the local relation was tested, the consistency of the fluid substitution analysis is observed (the velocities predictions honored the Hashin-Shtrikman bounds). Although not as small as the erros associated with the reference-well, the test-wells' RMSE values are small enough to justify the application of a shear velocity estimation using the compressional velocity (for formations of known lithology and fluid saturation).

2.3.2.1   Verification on Viking Graben data

We performed a velocity estimation using the calibrated relations (presented at Figure 2.7) on a well-log dataset from the northern North Sea basin, more specifically the North Viking Graben. In this field, many of the hydrocarbon reservoirs are located in the Middle Jurassic sandstones, which present complex geology (heavily faulted and overpressured zones). The analysis conducted on this well consisted of verifying the quality of fitting when using empirical relations derived from other data. First, it can be noted that the predicted logs on Figures 2.11a and 2.11b fitted the measured S-wave velocity log with similar quality, revealing a better estimation by the relations calibrated from the Norne Field data (red curve at Figure 2.11c). However, the RMSE values obtained on this validation data indicate a lower fitting quality than the predictions observed on the Norne test wells B and C. Although the Viking Graben and the Norne region have geological properties in common, this accuracy difference supports the fact that local relations should be derived if a larger dataset is available.
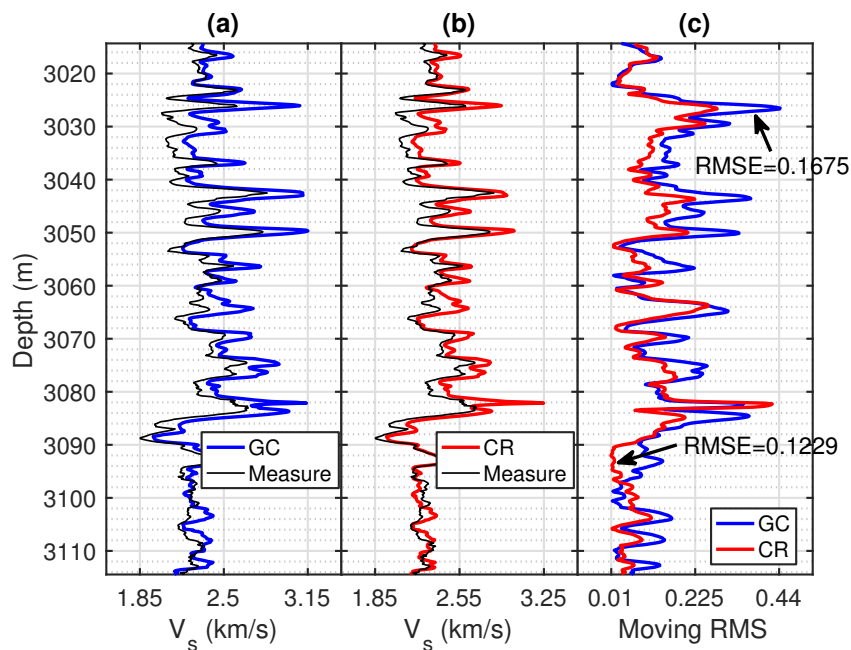
Figure 2.11: Results of V_S prediction on the Viking Graben data using (a) Greenberg-Castagna (GC) and (b) the calibrated relations (CR). At (c) there are error distributions of the two predicted logs in relation to the measured shear velocity.

Here it is important to mention that equations derived from regression coefficients, but non-polynomial models, were used by De Sousa et al. (2015) to estimate V_S for the Norne field. There, the first decimal point (in km/s) was questionable for some logs and, therefore, presented lower precision than that achieved with the hybrid model discussed here. In this context, the use of hybrid models, which takes into account lithology and saturation levels, is undoubtedly an effective alternative to find empirical relations of V_S as a function of V_P.

2.4   CONCLUSIONS

Whether of theoretical, empirical or heuristic nature, several physical-mathematical models were developed with the purpose of creating alternatives to obtain the S-wave information from parameters better measured by well-logging tools. The V_P-V_S relations are a fundamental instrument in this context, because this pair of attributes allows us a better understanding of the dynamics of a reservoir, describing from lithological aspects to geomechanical features. The combination of the empirical factor with the theoretical aspect studied in the present work (adapting the model of Greenberg and Castagna (1992)) led to a hybrid model that, although restricted to the situation where there is information about lithology and fluid saturation, showed strong predictive efficiency, fulfilling the role of S-wave velocity estimator.

The feasibility of our results was demonstrated through the hybrid method application in logs of three wells. For all the Norne studied wells, the root-mean-square error (RMSE) between the real value and the estimated by the empirical formulations was lower for our calibrated relation than for the conventional Greenberg-Castagna equation. Moreover, the model application on the Viking Graben data resulted in a loss of fitting quality in comparison to the Norne predictions, but still better than Castagna et al. (1993)'s relations. This results are further confirmation that the Greenberg-Castagna relation should be adapted for each formation where it is being used.

As mentioned previously, in most cases, empirical equations are efficient to estimate V_S (with limitations), even in cases when not all petrophysical parameters are available. The application and use of S-wave information extends from seismology to hydrocarbon reservoir characterization. From the Rock Physics point of view, V_P/V_S ratio is an important ingredient to tell us indirectly about matrix material, state of saturation, degree of consolidation, pore geometry, etc. In the best case scenario, where it is possible to acquire shear wave sonic data, there is a real chance that the data needs to be regularized (to reduce seismic interpretation risks), another reason why such calibrated empirical models are important.

We believe that one limitation of this work is the application of this methodology for carbonate reservoir. The application of conventional effective medium theories (Voigt-

Reuss-Hill or Hashin-Shtrikman) and fluid substitution theories (such as Gassmann or Biot) on carbonate environments show many pitfalls. A generalization that we suggest as a future work would be to perform this analysis using effective medium theories that take into account a background medium with heterogeneities. For this proposal, we suggest the use of theories such as the Differential Effective Medium (DEM) or the Self-Consistent Theory (SCT) coupled with Gassmann or Biot equations (or others fluid substitution theories for heterogeneous media, e.g. Brown-Korringa).

3 ARTICLE 2 - INTERVAL MINERAL AND FLUID DENSITIES ESTIMATION FROM WELL-LOGS: APPLICATION TO THE NORNE FIELD DATASET

Matias C. de Sousa, José J. S. de Figueiredo, Cicero R. T. Régis and Carolina B. da Silva

Formation evaluation techniques are the key to understand subsurface rocks properties from well-logs, especially those drilled in hydrocarbon exploration wells. Knowledge of the parameters related to different types of rocks is traditionally used in forward determination of lithology, porosity and water saturation, which can be refined by calibrating the input models. In this work, we perform well-log interval linear inversion with respect to formation density in a real case. The method is based on a highly overdetermined problem, which assumes a homogeneous distribution of petrophysical parameters through stratigraphic units and is applied in conventional reservoir rocks from the Norne Field (offshore Norway). Bulk density, gamma-ray and neutron porosity logs are employed in a workflow that relies on layer-by-layer least-squares regressions to estimate matrix, shale and fluid apparent densities, considering shale volume and porosity empirical calculations from the input logs. Furthermore, the application in two wellbores resulted in geological consistent individual densities in most intervals, except for a gas-bearing zone observed in one of the boreholes, where porosity uncertainty caused anomalous variation in grain and fluid densities.

3.1 INTRODUCTION

Extracting lithology and pore fluid information from well-log data is essential to hydrocarbon exploration. Sonic, density and neutron measurements are routinely used for this task, for example, because they exhibit a strong porosity dependence and still hold some sensitivity to rock matrix as discussed by Ellis and Singer (2007). Density-sonic, neutron-sonic, neutron-density, matrix identification (MID) and other cross plotting methods consist in well-known interpretation tools for lithology determination, which are useful to obtain preliminary estimations of reservoir rocks composition (Ijasan et al., 2013; Schlumberger, 2013). These graphical techniques, however, are improper for complex formations (multimineralic rocks, thinly bedded, invaded formations, etc). In these cases, numerical approaches can be applied to investigate the mineral constituents and formation fluids from well-logs, such as neural networks and fuzzy logic, which are commonly used to map electrofacies (Cuddy, 1997; Maiti et al., 2007; Bosch et al., 2013; Correia

and Schiozer, 2016). Furthermore, deterministic linear inversion of petrophysical logs is widely used to compute volumetric concentrations of assumed rock mineral and fluid constituents, considering that there are linear relationships between these concentrations and formation properties such as density, porosity and sonic traveltimes (Mayer, 1980; Doveton, 1994; Heidari et al., 2012; Heidari et al., 2013).

The bulk density (ρ_b) is extremely important to the mentioned formation evaluation methods, it is a rock property that can be accurately measured in the borehole environment by logging tools based on gamma ray scattering and the formation electron density response, or obtained from laboratory core analysis (Schön, 2015; Tiab and Donaldson, 2015). Density also contributes to the seismic response of subsurface rocks, nevertheless, it is not direct obtained from seismic data and usually requires to be estimated based on empirical models, such as the equations derived by Gardner et al. (1974) and Lindseth (1979). In petrophysics, the total porosity of rocks can be obtained from the formation density and then applied into core-log correlations and Archie (1942)'s law to estimate, respectively, permeability and fluid saturations (Nelson, 1994; Kennedy, 2015). From the seismic point of view, the product of density and velocity (impedance) describes subsurface layers' contrast and is used to build earth's reflectivity series, perform AVO (amplitude variation with offset) and well-tie analyses (Castagna and Backus, 1993; Chopra and Castagna, 2014; Macedo et al., 2017). Moreover, pore pressure prediction requires density information to be achieved, specially to compute overburden stress (Zhang, 2011). Therefore, density plays an important role as a lithological descriptor in seismic calibration, petrophysics and geomechanics.

In siliciclastic rocks, the formation density can be properly described as a combination of three main densities: matrix (ρ_{ma}), shale (ρ_{sh}) and fluid (ρ_{fl}). There are different approaches to estimate these individual densities from well-logs. Maiti et al. (2007) using neural network modelling and Bosch et al. (2013) using the logical fuzzy method estimated (indirectly) the main mineral on reservoir regions. In those works, the main goal was to perform a qualitative analysis of lithofacies. Heidari et al. (2012), on the other hand, introduced a non-linear joint inversion method to quantify the individual layer properties of thinly bedded and invaded formations, that then was extended to carbonates (Heidari et al., 2013). The conventional inversion methods for lithology evaluation focus on determining local volumetric concentrations of these constituents, assuming prior knowledge of the individual densities. In contrast, here is employed an alternative linear inversion approach to estimate interval values of ρ_{ma}, ρ_{sh} and ρ_{fl}, that considers prior information about volumetric concentrations derived from petrophysical logs (gamma-ray and ρ_b). Applying the well-logging inversion procedure in a longer processing interval allows more accurate solutions since the overdetermination ratio of the problem increases (Dobróka and Szabó, 2001; Dobróka et al., 2016). Furthermore, we performed pre-analyses in a real dataset from the Norne Field in order to determine precise density estimations for the

studied reservoir zones and verify the feasibility of ordinary least-squares solutions in this well-logging inversion.

3.2 METHODOLOGY

The statistical estimation of mineral and fluid densities is established from an assumption that is also valid in conventional deterministic well-logs inversion methods: there are representative linear models between volumetric concentrations and individual properties of each petrophysical constituent (Mayer, 1980). For multimineralic rocks the bulk density is expressed by the linear relation

$$\rho_b = \sum_{i=1}^{n} v_i \, \rho_i \,, \tag{3.1}$$

where v_i and ρ_i are the volumetric fraction and the individual density of the i-th constituent (n phases, including pore fluids), respectively. This model is known as a general density mixing law that can be used to calculate the density of different types of rocks and makes possible to simulate ρ_b logs. As remarked by Vernik (2016), these individual densities are representative of a rock layer in situ if the formation is laterally homogeneous on at least a 0.25 m scale and vertically homogeneous on at least a $0.5\,m$ to $0.75\,m$ scale, i.e., the volume around the wellbore wall is homogeneous regarding the depth of investigation and vertical resolution of density log. Sandstone matrix density from $2.64\,g/cm^3$ to $2.68\,g/cm^3$; limestone matrix of $2.71\,g/cm^3$; dolomite matrix density from $2.84\,g/cm^3$ to $2.9\,g/cm^3$; water-bearing formation fluid density from $0.95\,g/cm^3$ to $1.25\,g/cm^3$; and hydrocarbon-bearing formation fluid density from $0.1\,g/cm^3$ to $1\,g/cm^3$ are typical ranges/values assumed in these calculations (Kennedy, 2015). Adopting grain density for shales is a more complex task due to the wide range of clay minerals.

In this paper we assume a siliciclastic hydrocarbon-bearing rock model that consists of a solid matrix, shale and pore fluids. Thus, the particular case of equation (3.1) that describes clastic reservoirs is written as

$$\rho_b = (1 - v_{sh} - \phi) \, \rho_{ma} + \phi \, \rho_{fl} + v_{sh} \, \rho_{sh} \,, \tag{3.2}$$

where v_{sh} and ϕ are the shale volume and the effective porosity, respectively. The volumetric fractions of mineral and fluids can be calculated depth-by-depth using volume weighted models of various well-logs (e.g. neutron porosity and sonic traveltime). However, these deterministic methods require reliable log responses across pure lithologies and fluids to define the individual properties. Instead of solving simultaneously several linear equations to estimate mineral and fluid weighted fractions from different log responses (multivariate regression), the present work focus on finding a least-squares solution to

equation (3.2) for a set of bulk density readings in layer interval, considering known local relations between well-log measurements that provide proper inputs of v_{sh} and ϕ for the studied wells, as well as a consistent reservoir zonation. In the following sections are detailed important data processing steps and the least-squares fitting procedure used to estimate layer-by-layer values of ρ_{ma}, ρ_{sh} and ρ_{fl}.

3.2.1 Data preparation

The interval inversion workflow relies on three imperative well-logs to perform formation evaluation: ρ_b, gamma-ray (GR_{log}) and neutron porosity (ϕ_n). The first two are direct employed to quantify mineral and fluid densities, while the third is used as an interpretation parameter (explication of anomalous density predictions). The logging tools that record these subsurface properties in wellbores are exposed to several factors that might contaminate the data with noise, such as instrument error, borehole conditions and human error. In order to reduce the noise in the data we adopted the statistical technique proposed by Tukey (1977), that allows the detection and removal of outliers, which are observations that deviate far from the mean data value. This method considers two reference samples with respect to dataset range divided into four equal-sized groups: the first (Q_1) and the third (Q_3) quartiles. Q_1 is defined as the middle number between the smallest number and the median of the dataset, whereas Q_3 is the middle value between the median and the highest number. In practice, they are the medians of lower and upper halves of a dataset, which means that about 25% of the measures are below Q_1 and 25% above Q_3. The interquartile range (IQR) can describe the data when there are possible extremities that distort it and is calculated by applying the quartiles in the following expression:

$$IQR = 1.5\left(Q_3 - Q_1\right). \tag{3.3}$$

These statistical parameters are then used to identify as an outlier any measurement outside the interval $[Q_1 - IQR, Q_3 + IQR]$, which is called Tukey's fences. Removing this kind of data samples is useful to improve the correlation between the input logs.

After studying the statistical features and filtering the outliers in the well-logs, the next step of data preparation consisted in the calculations of rock volumetric fractions using empirical approaches. First, the gamma-ray index (I_{GR}) is obtained applying the relation

$$I_{GR} = \frac{GR_{log} - GR_{min}}{GR_{max} - GR_{min}}, \tag{3.4}$$

where GR_{min} is the mean minimum gamma-ray measurement, usually computed trough clean sandstones or carbonates, and GR_{max} is the mean maximum gamma-ray value typically observed trough shales. Although the normalization of GR_{log} result a function strong dependent on shale volume, assuming a linear relation between I_{GR} and v_{sh} may

lead to overestimations. The gamma-ray index log must be corrected according to rock age using the following non-linear relationship:

$$v_{sh} = a\left(2^{b\,IGR} - 1\right),\tag{3.5}$$

where a and b are empirical coefficients. Larionov (1969) evaluated these coefficients for Tertiary (unconsolidated) rocks and for older (consolidated) rocks. For Jurassic formations a and b are, respectively, 0.33 and 2. In addition to shale volume, we calculated the effective porosity from ρ_b using the linear model

$$\phi_d = c + d\,\rho_b,\tag{3.6}$$

where the coefficients c and d are estimated from core-log correlations (Yan, 2002) for each formation in the Norne Field case.

3.2.2 Density multiple linear regression

The functional model (3.2) would provide an exact value of ρ_b only if the set of parameters ϕ, v_{sh}, ρ_{ma}, ρ_{fl} and ρ_{sh} are exactly measured. Even though good noise reduction techniques are employed, such as outliers removal, it is natural that real datasets hold measurement errors. An statistical model is one that acknowledges such errors. Rewriting the weighted density law, a multiple linear regression model of 2 independent predictor variables (ϕ_d and v_{sh}) is defined:

$$\rho_b = x_0 + x_1\,\phi_d + x_2\,v_{sh} + r,\tag{3.7}$$

where the regression coefficients x_0, x_1 and x_2 are equivalent to matrix density, the difference between fluid and matrix densities and the difference between shale and matrix densities, respectively. From a collection of n data points, the residuals r_i between bulk density observations and modeled density can be written as

$$\underbrace{\begin{bmatrix} r_1 \\ r_2 \\ \vdots \\ r_n \end{bmatrix}}_{r} = \underbrace{\begin{bmatrix} \rho_{b_1} \\ \rho_{b_2} \\ \vdots \\ \rho_{b_n} \end{bmatrix}}_{y} - \underbrace{\begin{bmatrix} 1 & \phi_{d_1} & v_{sh_1} \\ 1 & \phi_{d_2} & v_{sh_2} \\ \vdots & \vdots & \vdots \\ 1 & \phi_{d_n} & v_{sh_n} \end{bmatrix}}_{A} \cdot \underbrace{\begin{bmatrix} x_0 \\ x_1 \\ x_2 \end{bmatrix}}_{x}.\tag{3.8}$$

To do invert this system the quantity of the measurements (n) must be greater than the number of independent variables (2), otherwise the problem becomes underdetermined and may need to be constrained using a priori information. We ensure that this problem is significantly overdetermined when chose to fit the well-logs through known reservoir

zones (greater than the depth sampling interval). Therefore, the individual densities can be estimated by solving the matricial equation (3.8) in a least-squares sense, i.e., computing x_0, x_1 and x_2 that minimize the sum of squared residuals. Thus, we adopted the ordinary least-squares estimator

$$\boldsymbol{x} = \left(\boldsymbol{A}^T \boldsymbol{A}\right)^{-1} \boldsymbol{A}^T \boldsymbol{y}\,, \tag{3.9}$$

which is the solution to the problem formally expressed by

$$\min_{x} \|\boldsymbol{y} - \boldsymbol{A}\boldsymbol{x}\|_2^2\,, \tag{3.10}$$

where superscript T indicates the matrix transpose and $\|\cdot\|_2$ denotes the L-2 or Euclidean norm. In the end, interval mineral and fluid densities are obtained from the regression coefficients computed by equation (3.9), taking into account the simple algebraic operations used to transform model (3.2) into (3.7), as shown in the last output in Figure 3.1. In the next section are presented the results obtained by applying this inversion approach in a real dataset.
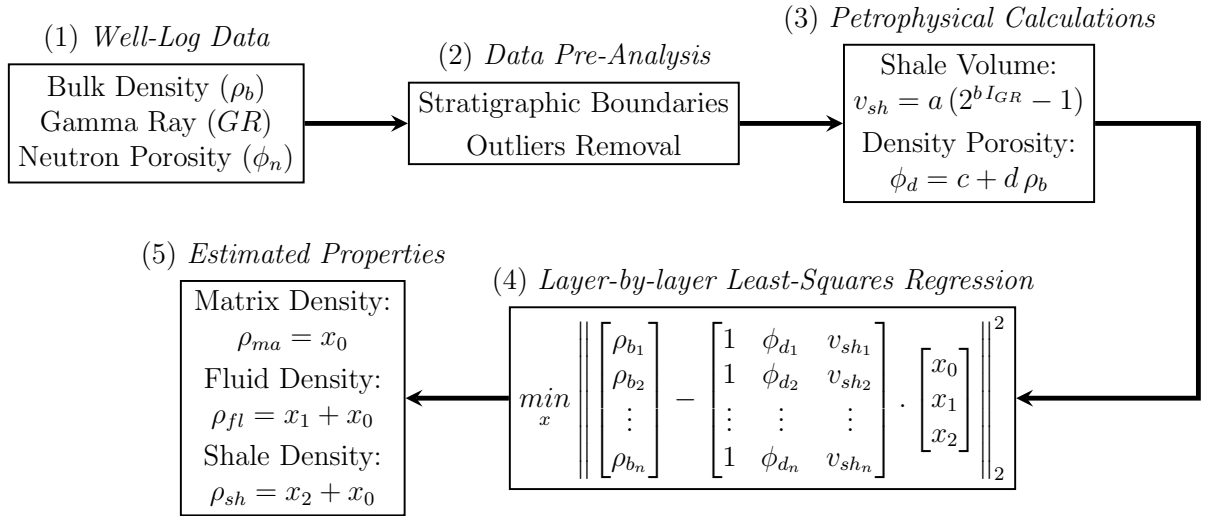
Figure 3.1: Workflow adopted in this study. The input well-logs (1) are pre-processed in depth intervals of reservoir zones that are delimited according to geological information (2). Based on empirical relations, the volumetric fractions are calculated (3). For each reservoir layer the density multiple linear model is solved on a least-squares sense (4), that results estimations of matrix, fluid and shale densities (5).
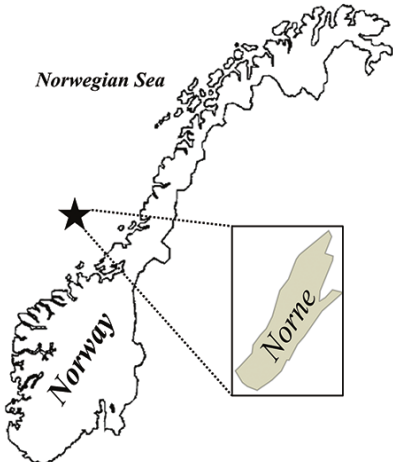
3.3   RESULTS AND DISCUSSION

The dataset used in this work comprises well-logs from the Norne Field benchmark case, which are provided by Statoil and managed by the Norwegian University of Science and Technology (NTNU). Formed as a result of Permian and Late Jurassic - Early Cretaceous rifting episodes, the Norne Field is located in the mid-Norwegian Sea, specifically

on a flat horst block in the Norwegian continental shelf (Rwechungura et al., 2010). The field preserved hydrocarbons in Middle and Early Jurassic sandstones consolidated from post-rift sediments deposition, which includes reservoir zones subdivided into the Garn, Ile, Tofte and Tilje Formations. The Not Formation acts as a barrier between the adjacent zones (Garn and Ile) due to its shale sealing properties. Additionally, as outlined in Figure 3.2, there are a shale (Melke Formation) and a heterolithic sandstone interbedded with mudstones, shale and coals (Åre Formation) that delimit the reservoir, the first behaving as the cap rock and the second as the reservoir basal rock. More descriptions about Norne stratigraphy are detailed in Dalland et al. (1988) and Swiecicki et al. (1998).

We applied the interval density estimation in two Norne wellbores (6608/10-C-3H and 6608/10-E-3H), which here are named Well A and Well B. The available data include gamma-ray, bulk density and neutron porosity well-logs, as well as derived logs of density porosity and shale volume. Porosity calculations considering water-based mud (WBM) system were performed using equation (3.6), taking into account coefficients (c and d) obtained from cross-plots of overburden-corrected core porosity vs. density log (Verlo and Hetland, 2008). The well zonation was adopted following the Statoil (2001)'s report, which considered 15 zones based on combined sequence stratigraphic and lithostratigraphic criteria via core and biostratigraphic information.

In Table 3.1 is displayed the distribution of the depth intervals for both wells, considering the top of Åre Formation as the reservoir base. Moreover, there are measured depth variations between the boreholes because Well A was drilled in the southern region of the field, whereas Well B was perforated in the northerly Norne segment. Increased erosion to the north of the field makes the reservoir thickness to vary from to 267.9 m to 188.4 m, especially affecting Ile and Tilje formation heights.

Norne stratigraphy		
Age		Formation
Jurassic	Mid	Melke
		Garn
		Not
		Ile
	Early	Tofte
		Tilje
		Are

Figure 3.2: Norne Field location and sequence of geological formations. Garn, Ile, Tofte and Tilje comprise the main reservoir zones (modified from Maleki et al. (2018)).

Table 3.1: Reservoir zonation of the investigated wells (Statoil, 2001). The stratigraphic tops (expressed in m) are in Measured Depth (MD) and layer thicknesses in True Vertical Depth (TVD).

Zone	Well A		Well B	
	Top MD	Thickness TVD	Top MD	Thickness TVD
$Garn_3$	3348	6.9	2706.5	9.2
$Garn_2$	3355.2	10.6	2716	14.5
$Garn_1$	3366.2	10.8	2731	10.6
Not	3377.4	10.2	2742	6.7
Ile_3	3388	26.1	2749	15.4
Ile_2	3415	21.1	2765	6.3
Ile_1	3436.8	3.2	2771.5	3.4
$Tofte_4$	3444	7.3	2775	9.6
$Tofte_3$	3447.5	30.6	2785	28.3
$Tofte_2$	3479	8.3	2814.5	5.3
$Tofte_1$	3487.5	15.1	2820	13.4
$Tilje_4$	3503	25.3	2834	2.4
$Tilje_3$	3529	24.4	2836.5	16.7
$Tilje_2$	3554	46.1	2854	30
$Tilje_1$	3601.2	32.1	2885.5	23.3
Åre	3634	-	2910	-

In Figure 3.3 are shown ρ_b, GR and ϕ_n well-logs used in the lithological quantification process. The solid black curves corresponds to the raw data which were subjected to the Tukey's method in order to reduce the noise before performing the inversion. We evaluated the Tukey's fence for each reservoir zone to identify outliers and discard its respective data points, depicted as red crosses in Figure 3.3. Initially, there were 2287 and 1629 samples in Well A and Well B, respectively. In this same order, 168 and 121 data points were detected and eliminated. Most amount of outliers was related to the bulk density readings, while gamma-ray accounts for a small portion of them. These two logs (ρ_b and GR) affects directly the density regression outcomes, thereby we expected that the correlations among the petrophysical fractions (v_{sh} and ϕ_d) and formation density increase after this data pre-processing. The variation of those correlations are presented in Table 3.2, wherein the strong dependence between ρ_b and ϕ_d is verified for both wells (coefficient of determination R^2 higher than 0.98). Also, we noted that approximately 40% of bulk density variability is explained by v_{sh} (R_a^2 values of 0.4032 and 0.3921). Neutron porosity readings are important to interpret possible effects of rock composition in the estimated densities, albeit not employed in the minimization problem.
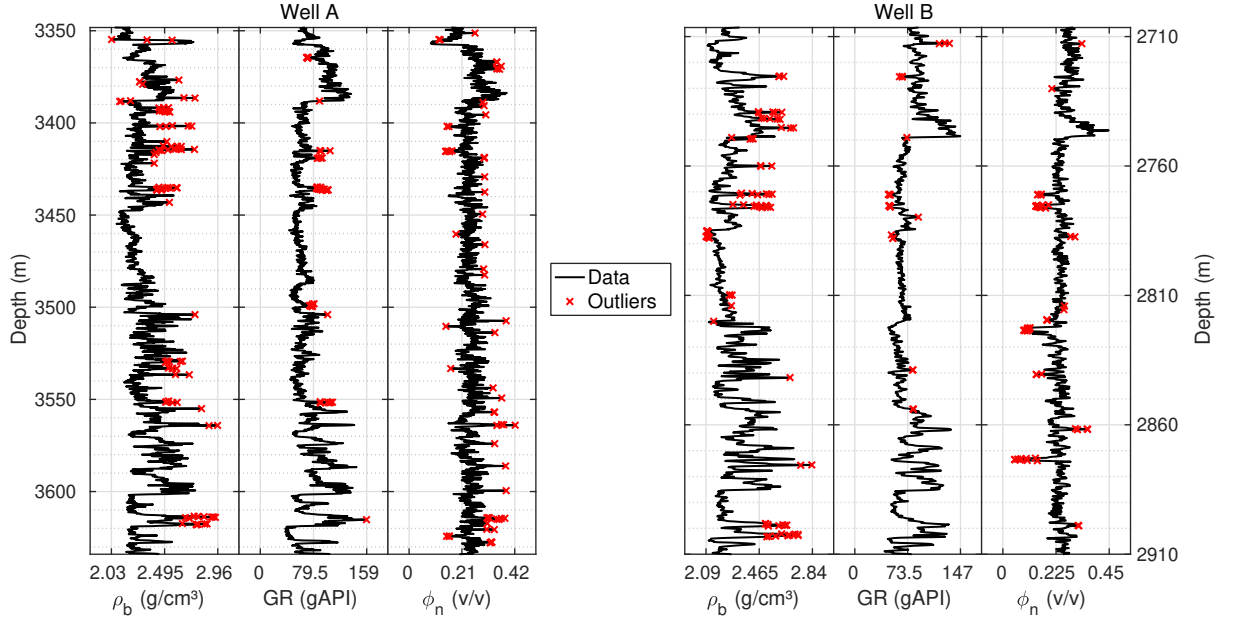
Figure 3.3: Well-logs in the reservoir intervals of each studied well. Tracks per well (from left to right): bulk density, gamma ray and neutron porosity. The outliers identified for each reservoir zone indicates data points that were discarded for the inversion procedure.

Table 3.2: Observed model (bulk density) response to shale volume and density porosity before (R_b^2) and after (R_a^2) outliers removal (in terms of coefficient of determination).

Log	Well A		Well B	
	R_b^2	R_a^2	R_b^2	R_a^2
ϕ_d	0.9752	0.9868	0.9868	0.9872
v_{sh}	0.3851	0.4032	0.3204	0.3921

The estimated interval matrix, fluid and shale densities are presented in a log form in Figures 3.4 and 3.5. A first look into the results indicates a notable accuracy of the proposed density model (minimal residuals per layer), except for the top Garn zone in Well A, where perhaps the rock properties weren't properly evaluated (upper layer in Figure 3.4). A fluid density of $1.53\,g/cm^3$ was obtained for the top of Garn Formation, which is quite unrealistic in terms of rock porous composition, since the most dense brines reach $1.4\,g/cm^3$ of density. In Garn$_3$ zone, the estimated shale density of $2.39\,g/cm^3$ can be accounted for kaolinite composition, but matrix density of $2.43\,g/cm^3$ is too low for sandstones. However, there is a significant difference between ϕ_n and ϕ_d in this interval, which can be related to gas-saturated pores and, hence, explains why the computed individual properties aren't representative of the wellbore near formations. Also, the bulk density log is more affected by mud-filtrate invasion in a gas reservoir drilled with water-based mud due to the large density contrast between the formation fluid and the mud-filtrate.
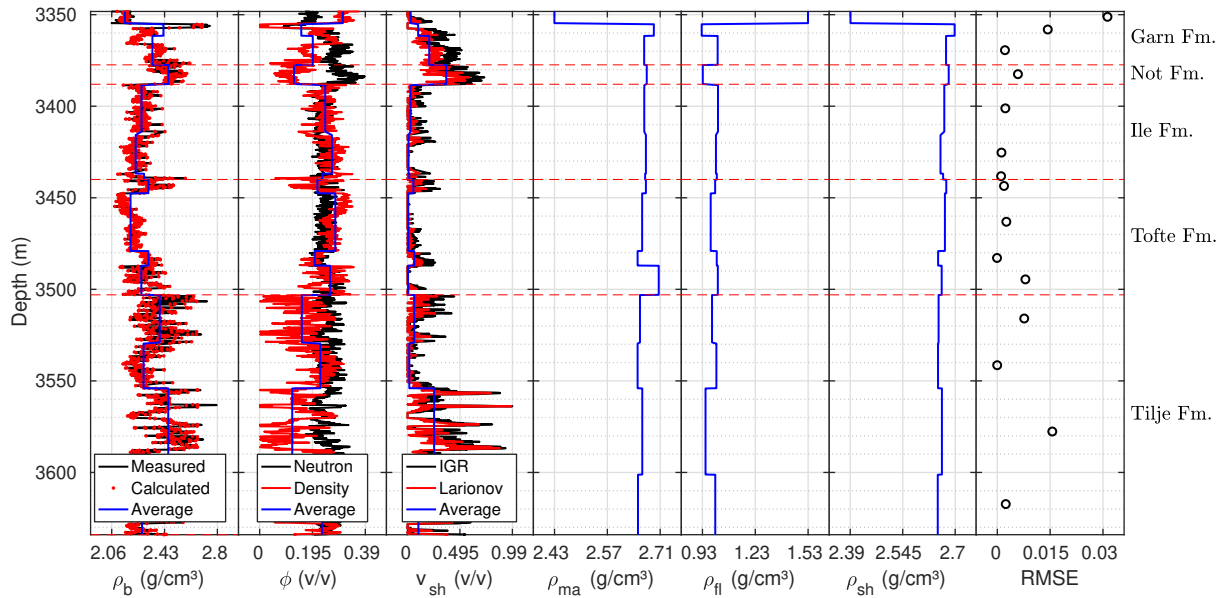
Figure 3.4: Input well-logs and interval estimated properties for Well A: formation density, porosity, shaliness, matrix density, fluid density and shale density. In the last track are the misfits for each interval, in terms of root-mean-squared error.
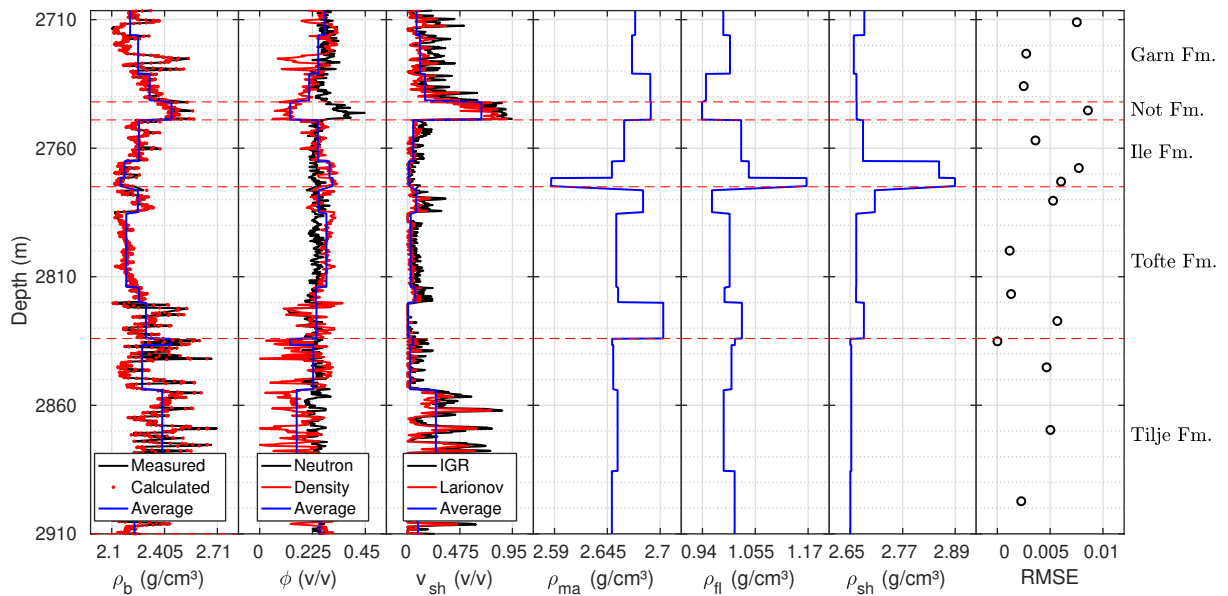
Figure 3.5: Input well-logs and interval estimated properties for Well B: formation density, porosity, shaliness, matrix density, fluid density and shale density. In the last track are the misfits for each interval, in terms of root-mean-squared error.

Another set of interval densities diverged from the estimations in Well B, on the base of Ile Formation. Ile_1 is a thin layer of $3.4\,m$ (see Table 3.1), where ρ_{ma}, ρ_{fl} and ρ_{sh} estimates of $2.59\,g/cm^3$, $1.17\,g/cm^3$ and $2.89\,g/cm^3$ were calculated, respectively. These densities indicate a brine-saturated layer, with quartz/feldspar matrix and dense clay minerals (glauconite/chlorite). The estimated shale density in Ile_2, above of Ile_1, also corresponds to dense clay minerals ($2.85\,g/cm^3$), whilst the matrix and fluid are related

to quartz $(2.65\,g/cm^3)$ and water $(1.04\,g/cm^3)$. In Table 3.3 are shown the density values estimated in the investigated wells.

Table 3.3: Interval density estimates and average fractions per zone. Densities in g/cm^3.

Zone	Well A					Well B				
	ρ_{ma}	ρ_{fl}	ρ_{sh}	ϕ_d	v_{sh}	ρ_{ma}	ρ_{fl}	ρ_{sh}	ϕ_d	v_{sh}
Garn$_3$	2.43	1.53	2.39	0.31	0.03	2.67	0.99	2.68	0.28	0.08
Garn$_2$	2.69	0.93	2.70	0.15	0.10	2.67	1.00	2.66	0.25	0.11
Garn$_1$	2.67	1.02	2.67	0.20	0.21	2.69	0.95	2.66	0.21	0.16
Not	2.67	0.93	2.68	0.12	0.37	2.69	0.94	2.66	0.13	0.67
Ile$_3$	2.67	1.02	2.67	0.24	0.02	2.66	1.02	2.68	0.25	0.05
Ile$_2$	2.67	1.01	2.66	0.27	0.01	2.65	1.04	2.85	0.30	0.01
Ile$_1$	2.67	1.01	2.66	0.23	0.02	2.59	1.17	2.89	0.31	0.02
Tofte$_4$	2.67	1.00	2.67	0.21	0.06	2.68	0.96	2.71	0.25	0.08
Tofte$_3$	2.66	0.98	2.67	0.28	0.01	2.65	1.00	2.66	0.28	0.03
Tofte$_2$	2.65	1.01	2.65	0.20	0.06	2.66	0.99	2.66	0.24	0.08
Tofte$_1$	2.71	1.02	2.66	0.26	0.01	2.70	1.03	2.68	0.24	0.01
Tilje$_4$	2.66	0.98	2.65	0.16	0.06	2.65	1.01	2.65	0.13	0.05
Tilje$_3$	2.65	1.01	2.65	0.22	0.02	2.65	1.00	2.65	0.23	0.02
Tilje$_2$	2.66	0.95	2.66	0.12	0.25	2.66	0.99	2.65	0.16	0.26
Tilje$_1$	2.65	1.00	2.65	0.23	0.10	2.65	1.01	2.65	0.25	0.09

Figures 3.6 and 3.7 show the density multiple regression outcomes for each formation in the studied wellbores, correlating the data to the shale content in the reservoir rocks. The quality of fitting was more significant in Well B, where the calculated bulk density (ρ_b^{cal}) accuracy is verified in the RMSE values observed in each zone, which are less than 0.01 (misfits in Figure 3.5). In Well A, it can be noted some local dispersions in Garn and Tilje formations, where ρ_b^{cal} didn't fitted the data. The first case is related the aforementioned gas effect in the derived logs in Garn$_3$, which led to overestimations for low ρ_b^{obs}. There are some underestimations for high bulk density values, which can be associated to a ρ_b spike near the interface of Garn$_3$ and Garn$_2$ ($3356\,m$) (see Figure 3.4). In Tilje Formation (Well A) bulk density was underestimated for the same reason, there are ρ_b spikes in Tilje$_4$ ($3505\,m$) and Tilje$_2$ ($3555\,m$), the first located in a clean reservoir zone and the second in a shaly zone. In general, the model fitted the data with a good accuracy, specially in Ile and Tofte reservoir zones, where v_{sh} is minimum and and ϕ_d is maximum (see Table 3.3).

According to Rwechungura et al. (2010), about 80% of Norne Field oil is located at Ile and Tofte formations, which has good reservoir properties such as the high pore volume we observed in wells A and B. Reservoir intervals of good quality are also found in upper part of Tilje and lower part of Garn formations, however, these zones are more laminated and cemented (Verlo and Hetland, 2008). There are calcareous cemented layers within Norne formations that explain some apparent matrix density values obtained through the

interval inversion, which trends to $2.71\,g/cm^3$ (calcite density). Furthermore, the diage-netic interval of Norne reservoir indicates that the subsurface formations were subjected to the transition from mechanical to chemical compaction, wherein clay minerals layering (e.g. illite, smectite and kaolinite) may be accounted for gradual increases in ρ_{sh} (Correia and Schiozer, 2016; Vernik, 2016).

Figure 3.6: Cross-plots of observed versus calculated bulk density for each formation of Well A. The data is color scaled according to shale volume. Clean zones are mainly found in Ile and Tofte formations.
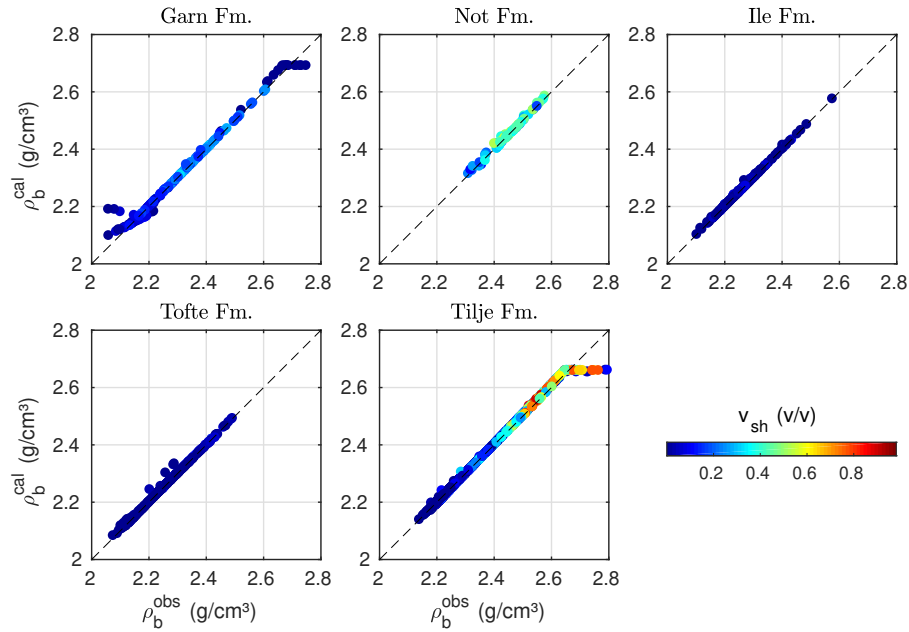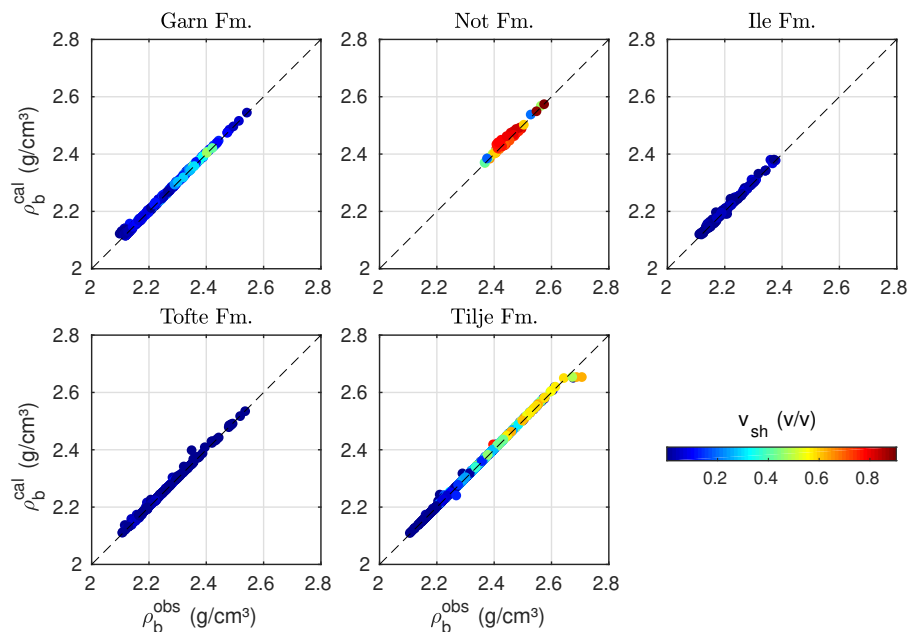

Figure 3.7: Cross-plots of observed versus calculated bulk density for each formation of Well B. The data is color scaled according to shale volume. Not and Tilje formations contains most argillaceous zones.

Analyzing the entire inversion results of Well A and Well B, it can be verified that the combination of quartz grains and mixed-layer clays can explain the density of the solid content of the studied formations, whereas water density can be accounted for the pore content. Figure 3.8 shows the occurrence of individual densities calculated along the defined zones for both wells. Interval density of $2.67\,g/cm^3$ (Well A) and $2.65\,g/cm^3$ (Well B) are the most frequent matrix property. For shale, most of density counts range from $2.65\,g/cm^3$ to $2.67\,g/cm^3$ (Well A) and $2.66\,g/cm^3$ (Well B). On the other hand, interval ρ_{fl} estimates don't properly reveal hydrocarbon saturation, albeit minimum values of $0.93\,g/cm^3$ (Well A) and $0.94\,g/cm^3$ (Well B) can be related to effective density of oil-water mixture. Concentrations of hydrocarbon combined with formation water yield an apparent fluid density that is expressed by

$$\rho_{fl} = S_w\,\rho_w + S_{hc}\,\rho_{hc} \tag{3.11}$$

where S_w, S_{hc}, ρ_w and ρ_{hc} refers respectively to water saturation, hydrocarbon saturation, density of formation water and density of reservoir hydrocarbon (the saturations sum to unity, i.e., $S_{hc} = 1 - S_w$). Furthermore, equation (3.11) is a relative simple model that has some pitfalls associated to density and resistivity logs (e.g. mud-invasion effect prediction). These uncertainties in shale and fluid densities exist due to the homogeneity assumptions of the rock volume adjacent to borehole wall, which can be more affected by the mud-cake in reservoirs penetrated by contrasting mud systems and, hence, contaminate the measurements in a scale depending on the resolution of logging tools (Vernik, 2016).
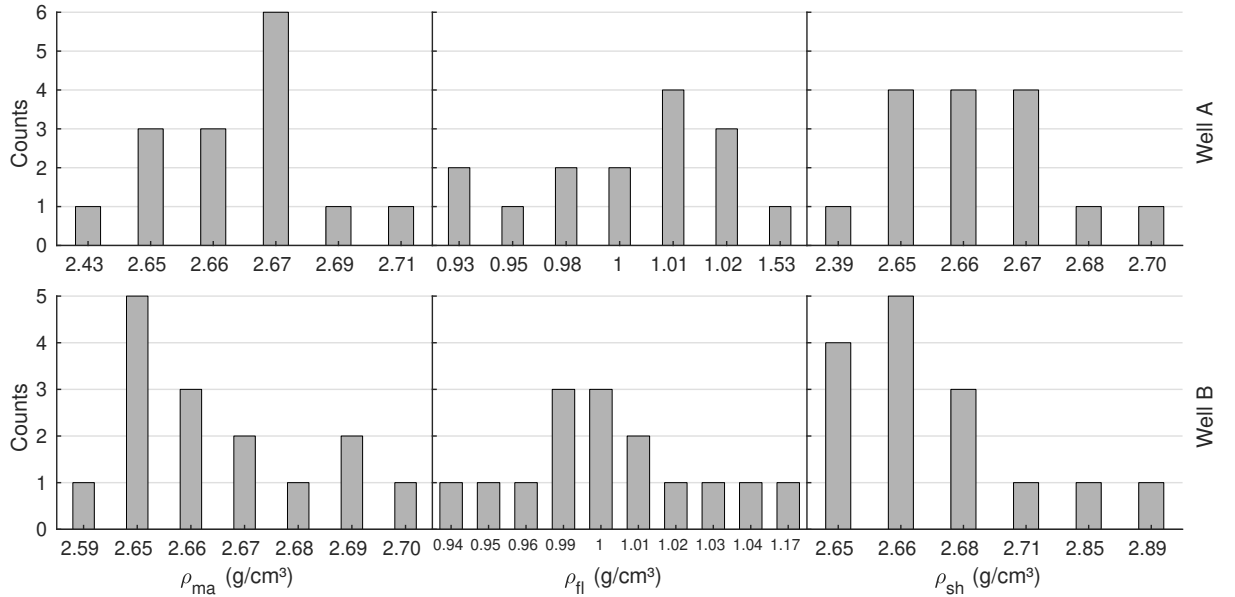
Figure 3.8: Frequency of estimated matrix, fluid and shale densities according to the Norne zonation for the investigated wells (15 zones).

3.4 CONCLUSIONS

The methods applied in formation evaluation conventionally estimate volumetric concentrations of rock constituents in different depth points separately, using several well-logs and assuming rock-frame properties. As we proposed in this study, the well-logging inversion problem can be approached using an ordinary least-squares estimator to evaluate interval densities of solid and pore volume constituents in a real dataset. Although this methodology has some limitations, we noted that the density multiple linear regression led to accurate solutions (misfits average lower than 0.03) that are mostly in accordance to downhole geology in the investigated wells. Gas saturation and mud-invasion effects are particular drawbacks of this interval procedure, since density measurements may not be representative of homogeneous media along the borehole zones in such conditions.

In general, the method was able to provide reliable estimates of layer individual densities based on prior information about Norne Field stratigraphic boundaries and volumetric fractions (derived from empirical relations). The purport of our interval inversion application was to perform a simple petrophysical evaluation of formation density of known reservoir zones, nonetheless, there are more complex procedures that employ joint inversion of well-logs to estimate both petrophysical parameters and formation boundaries. It would be interesting to jointly invert bulk density with electrical resistivity, sonic and nuclear logs when available. Therefore, we suggest the studied workflow for initial estimation of in situ rock layer properties, considering the great overdetermination of the interval approach as an important advantage to speed up the characterization of hydrocarbon reservoirs.

4 CONCLUSIONS

In the presented articles we investigated the estimation of two physical rock properties that primarily are used to evaluate the reservoir quality. First, this work focused on the determination of V_P-V_S equations that honor the mineral composition and the fluid content of downhole formations. Additionally, we considered the intrinsic linear relationship among the bulk density, the rock frame and pore fluids in order to estimate the density of the rock constituents, including its shale fraction. The accuracy of the shear wave velocity hybrid model and the goodness-of-fitting of the layerwise density inversion applied to the Norne Field dataset demonstrate that: (1) joint empirical correlations and model-based theories is an efficient tool for deriving petrophysical logs; (2) in addition to the notable dependence of rock effective properties on porosity (fluids), the perturbation on log responses caused by lithology (minerals) is properly accounted by volumetric rock models; and (3) the solutions obtained through ordinary least-squares estimator consist of a simple alternative to explain the well-logging data, which provides reasonable approximations to real reservoir properties.

In the dissertation, specially when discussing the density interval inversion case (in Chapter 3), we emphasized that the assumptions of the rock volumetric (layer) model are suitable to the borehole environment as long as the homogeneity of the formation adjacent to the wellbore wall is valid. In case the well measurements be affected by mud-invasion, gas saturation or complex lithologies, more constrained models may be required to explain the associated heterogeneities. Another observation that was highlighted in the shear velocity prediction case (in Chapter 2), is that the applied bounding methods and fluid substitution theory are free of assumptions about pore geometry and limited to isotropic, linear, porous and elastic media. Therefore, geometric petrophysical models (e.g. granular, capillary and inclusion types) and generalized formulation must be adopted to evaluate carbonate reservoir and unconventional resources.

We believe that the approached log-based workflows have the advantages of being quick and cost-effective alternatives to evaluate rock elastic properties. In practice, these parameters are combined to other well-logs and core data to provide information about porosity and hydrocarbon saturation, as well as on mechanical (e.g. elastic moduli and pore pressure) and mineralogical typing for completion evaluation. Furthermore, in future works it would be interesting to apply different log editing techniques for noise reduction (such as despiking), analyze other empirical correlations among petrophysical parameters (e.g. P-wave velocity to bulk density) and apply interval linear inversion to other properties measured in situ (such as P-wave traveltimes).

BIBLIOGRAPHY

Archie, G. E., 1942, The Electrical Resistivity Log as an Aid in Determining Some Reservoir Characteristics: Transactions of the AIME, **146**, 54–62.

Avseth, P., T. Mukerji, and G. Mavko, 2005, Quantitative Seismic Interpretation: Applying Rock Physics Tools to Reduce Interpretation Risk: Cambridge University Press.

Bagheripour, P., A. Gholami, M. Asoodeh, and M. Vaezzadeh-Asadi, 2015, Support vector regression based determination of shear wave velocity: Journal of Petroleum Science and Engineering, **125**, 95–99.

Biot, M. A., 1956, Theory of Propagation of Elastic Waves in a Fluid-Saturated Porous Solid. I. Low-Frequency Range: The Journal of the Acoustical Society of America, **28**, 168–178.

Biswas, R., and S. Baruah, 2016, Shear Wave Velocity Estimates through Combined Use of Passive Techniques in a Tectonically Active Area: Acta Geophysica, **64**, 2051–2076.

Bosch, D., J. Ledo, and P. Queralt, 2013, Fuzzy Logic Determination of Lithologies from Well Log Data: Application to the KTB Project Data set (Germany): Surveys in Geophysics, **34**, 413–439.

Brown, S., 1991, Stratigraphy of the oil and gas reservoirs: UK continental shelf, *in* United Kingdom oil and gas fields - 25 years commemorative volume: Geological Society, Memoirs, No. 14, 9–18.

Castagna, J., and M. Backus, 1993, Offset-Dependent Reflectivity—Theory and Practice of AVO Analysis: Society of Exploration Geophysicists, volume **8** *of* Investigations in Geophysics.

Castagna, J. P., M. L. Batlze, and T. K. Kan, 1993, Rock physics: The link between rock properties and AVO response, *in* Offset-Dependent Reflectivity-Theory and Practice of AVO Analysis: Society of Exploration Geophysicists, volume **8** *of* Investigations in Geophysics.

Castagna, J. P., M. L. Batzle, and R. L. Eastwood, 1985, Relationships between compressional-wave and shear-wave velocities in clastic silicate rocks: Geophysics, **50**, 571–581.

Chen, S., 1988, Shear-wave logging with dipole sources: GEOPHYSICS, **53**, 659–667.

Chen, S., 1989, Shear-wave logging with quadrupole sources: GEOPHYSICS, **54**, 590–597.

Cheng, A., 2015, Can we ever trust the shear-wave log?: The Leading Edge, **34**, 278–284.

Chopra, S., and J. Castagna, 2014, AVO: Society of Exploration Geophysicists, volume **16** *of* Investigations in Geophysics.

Correia, G. G., and D. J. Schiozer, 2016, Reservoir characterization using electrofacies analysis in the sandstone reservoir of the Norne Field (offshore Norway): Petroleum Geoscience, **22**, 165–176.

Cuddy, S., 1997, The Application Of The Mathematics Of Fuzzy Logic To Petrophysics: Presented at the SPWLA 38th Annual Logging Symposium, 15-18 June, Houston, Texas, Society of Petrophysicists and Well-Log Analysts.

Dalland, A., D. Worsley, K. Ofstad, Norway, and Oljedirektoratet, 1988, A lithostratigraphic scheme for the Mesozoic and Cenozoic and succession offshore mid- and northern Norway: Norwegian Petroleum Directorate Bulletin, **4**, 1–65.

De Figueiredo, J. J. S., J. Schleicher, R. R. Stewart, and N. Dyaur, 2012, Estimating fracture orientation from elastic-wave propagation: An ultrasonic experimental approach: Journal of Geophysical Research: Solid Earth, **117**, B08304.

De Sousa, M., J. De Figueiredo, and L. Santos, 2015, Estimativa de VS a partir de VP usando equações empíricas: 14th International Congress of the Brazilian Geophysical Society & EXPOGEF, Rio de Janeiro, Brazil, Brazilian Geophysical Society, 888–892.

Dobróka, M., N. Szabó, J. Tóth, and P. Vass, 2016, Interval inversion approach for an improved interpretation of well logs: GEOPHYSICS, **81**, D155–D167.

Dobróka, M., and N. P. Szabó, 2001, The inversion of well log data using Simulated Annealing method: Geosciences, Publications of the University of Miskolc, Series A (Mining), **59**, 115–138.

Doveton, J. H., 1994, Geologic Log Analysis Using Computer Methods: American Association of Petroleum Geologists, volume **2** *of* Computer Applications in Geology.

Dvorkin, J., and G. Mavko, 2014, VS predictors revisited: The Leading Edge, **33**, 288–296.

Ellis, D. V., and J. M. Singer, eds., 2007, Well Logging for Earth Scientists: Springer Netherlands.

Fertl, W. H., and H. H. I. Rieke, 1980, Gamma Ray Spectral Evaluation Techniques Identify Fractured Shale Reservoirs and Source-Rock Characteristics: Journal of Petroleum Technology, **32**, 2.053–2.062.

Gardner, G., L. Gardner, and A. Gregory, 1974, Formation velocity and density—the diagnostic basics for stratigraphic traps: GEOPHYSICS, **39**, 770–780.

Gassmann, F., 1951, Elastic waves through a packing of spheres: GEOPHYSICS, **16**, 673–685.

Gholami, J., A. Moradzadeh, V. Rasouli, and V. Hanachi, 2016, Shear Wave Splitting Analysis to Estimate Fracture Orientation and Frequency Dependent Anisotropy: Acta Geophysica, **64**, 76–100.

Gholami, R., A. Moradzadeh, V. Rasouli, and J. Hanachi, 2014, Shear wave velocity prediction using seismic attributes and well log data: Acta Geophysica, **62**, 818–848.

Gjerstad, H. M., l. Steffensen, and J. I. Skagen, 1995, The Norne Field - Exploration History & Reservoir Development Strategy: Presented at the Offshore Technology Conference, Offshore Technology Conference.

Glennie, K. W., and J. R. Underhill, 1998, Origin, Development and Evolution of Structural Styles, *in* Petroleum Geology of the North Sea, 4th ed.: Blackwell Science Ltd., 42–84.

Greenberg, M. L., and J. P. Castagna, 1992, Shear-Wave Velocity Estimation in Porous Rocks: Theoretical Formulation, Preliminary Verification and Applications1: Geophysical Prospecting, **40**, 195–209.

Han, D., A. Nur, and D. Morgan, 1986, Effects of porosity and clay content on wave velocities in sandstones: GEOPHYSICS, **51**, 2093–2107.

Hashin, Z., and S. Shtrikman, 1963, A variational approach to the theory of the elastic behaviour of multiphase materials: Journal of the Mechanics and Physics of Solids, **11**, 127–140.

Heidari, Z., C. Torres-Verdín, and W. Preeg, 2012, Improved estimation of mineral and fluid volumetric concentrations from well logs in thinly bedded and invaded formations: GEOPHYSICS, **77**, WA79–WA98.

Heidari, Z., C. Torres-Verdín, and W. E. Preeg, 2013, Improved estimation of mineral and fluid volumetric concentrations in thinly bedded carbonate formations: GEOPHYSICS, **78**, D261–D269.

Hill, R., 1963, Elastic properties of reinforced solids: Some theoretical principles: Journal of the Mechanics and Physics of Solids, **11**, 357–372.

Ijasan, O., C. Torres-Verdín, and W. E. Preeg, 2013, Interpretation of porosity and fluid constituents from well logs using an interactive neutron-density matrix scale: Interpretation, **1**, T143–T155.

Jorstad, A., T. Mukerji, and G. Mavko, 1999, Model-based shear-wave velocity estimation versus empirical regressions: Geophysical Prospecting, **47**, 785–797.

Kennedy, M., 2015, Practical Petrophysics: Elsevier, volume **62** *of* Developments in Petroleum Science.

Krief, M., J. Garat, J. Stellingwerff, J. Ventre, et al., 1990, A petrophysical interpretation using the velocities of p and s waves (full-waveform sonic): The Log Analyst, **31**.

Larionov, V., 1969, Borehole radiometry: Nedra, Moscow, **127**.

Lindseth, R., 1979, Synthetic sonic logs—a process for stratigraphic interpretation: GEOPHYSICS, **44**, 3–26.

Macedo, I. A. S. d., C. B. d. Silva, J. J. S. d. Figueiredo, and B. Omoboya, 2017, Comparison between deterministic and statistical wavelet estimation methods through predictive deconvolution: Seismic to well tie example from the North Sea: Journal of Applied Geophysics, **136**, 298–314.

Maiti, S., R. Krishna Tiwari, and H.-J. Kümpel, 2007, Neural network modelling and classification of lithofacies using well log data: a case study from KTB borehole site: Geophysical Journal International, **169**, 733–746.

Maleki, M., A. Davolio, and D. J. Schiozer, 2018, Qualitative time-lapse seismic interpretation of Norne Field to assess challenges of 4d seismic attributes: The Leading Edge, **37**, 754–762.

Mavko, G., C. Chan, and T. Mukerji, 1995, Fluid substitution: Estimating changes in VP without knowing VS: GEOPHYSICS, **60**, 1750–1755.

Mavko, G., T. Mukerji, and J. Dvorkin, 2009, The Rock Physics Handbook: Tools for Seismic Analysis of Porous Media: Cambridge University Press.

Mayer, C., 1980, Global, A New Approach To Computer-Processed Log Interpretation: Presented at the SPE Annual Technical Conference and Exhibition, 21-24 September, Dallas, Texas, Society of Petroleum Engineers.

Nelson, P. H., 1994, Permeability-porosity Relationships In Sedimentary Rocks: The Log Analyst, **35**.

Nourafkan, A., and A. Kadkhodaie-Ilkhchi, 2015, Shear wave velocity estimation from conventional well log data by using a hybrid ant colony–fuzzy inference system: A case study from Cheshmeh–Khosh oilfield: Journal of Petroleum Science and Engineering, **127**, 459–468.

Parvizi, S., R. Kharrat, M. R. Asef, B. Jahangiry, and A. Hashemi, 2015, Prediction of the Shear Wave Velocity from Compressional Wave Velocity for Gachsaran Formation: Acta Geophysica, **63**, 1231–1243.

Reuss, A., 1929, Berechnung der Fließgrenze von Mischkristallen auf Grund der Plastizitätsbedingung für Einkristalle.: ZAMM - Journal of Applied Mathematics and Mechanics / Zeitschrift für Angewandte Mathematik und Mechanik, **9**, 49–58.

Rezaee, M. R., A. Kadkhodaie Ilkhchi, and A. Barabadi, 2007, Prediction of shear wave velocity from petrophysical data utilizing intelligent systems: An example from a sandstone reservoir of Carnarvon Basin, Australia: Journal of Petroleum Science and Engineering, **55**, 201–212.

Rwechungura, R. W., E. Suwartadi, M. Dadashpour, J. Kleppe, and B. A. Foss, 2010, The Norne Field Case - A Unique Comparative Case Study: Presented at the SPE Intelligent Energy Conference and Exhibition, 23-25 March, Utrecht, The Netherlands, Society of Petroleum Engineers.

Røgen, B., L. Gommesen, and I. L. Fabricius, 2004, Methods of velocity prediction tested for North Sea chalk: a review of fluid substitution and vS estimates: Journal of Petroleum Science and Engineering, **45**, 129–139.

Santos, L. K., J. J. S. De Figueiredo, B. Omoboya, J. Schleicher, R. R. Stewart, and N. Dyaur, 2015, On the source-frequency dependence of fracture-orientation estimates from shear-wave transmission experiments: Journal of Applied Geophysics, **114**, 81–100.

Schlumberger, 2013, Log interpretation charts: Schlumberger.

Schön, J. H., 2015, Physical Properties of Rocks: Fundamentals and Principles of Petrophysics: Elsevier, volume **65** *of* Developments in Petroleum Science.

Statoil, 2001, PL128 - Norne Reservoir Management Plan: Technical report, HNO Norne PETEK.

Stevens, J. L., and S. M. Day, 1986, Shear velocity logging in slow formations using the Stoneley wave: GEOPHYSICS, **51**, 137–147.

Swiecicki, T., P. B. Gibbs, G. E. Farrow, and M. P. Coward, 1998, A tectonostratigraphic framework for the Mid-Norway region: Marine and Petroleum Geology, **15**, 245–276.

Tan, M., X. Peng, H. Cao, S. Wang, and Y. Yuan, 2015, Estimation of shear wave velocity from wireline logs in gas-bearing shale: Journal of Petroleum Science and Engineering, **133**, 352–366.

Tang, X. M., and T. Wang, 2005, Stress effects on wireline and logging-while-drilling shear-wave measurements and interpretation, *in* SEG Technical Program Expanded Abstracts 2004: 286–289.

Tiab, D., and E. C. Donaldson, 2015, Petrophysics: Theory and Practice of Measuring Reservoir Rock and Fluid Transport Properties: Elsevier.

Tokhmchi, B., H. Memarian, and M. R. Rezaee, 2010, Estimation of the fracture density in fractured zones using petrophysical logs: Journal of Petroleum Science and Engineering, **72**, 206–213.

Tukey, J. W., 1977, Exploratory Data Analysis: Addison-Wesley, volume **2** *of* Behavioral Science - Quantitative Methods.

Verlo, S. B., and M. Hetland, 2008, Development of a field case with real production and 4d data from the norne field as a benchmark case for future reservoir simulation model testing: Master's thesis, Norwegian University of Science and Technology.

Vernik, L., 2016, Seismic Petrophysics in Quantitative Interpretation: Society of Exploration Geophysicists, volume **18** *of* Investigations in Geophysics.

Vernik, L., D. Fisher, and S. Bahret, 2002, Estimation of net-to-gross from P and S impedance in deepwater turbidites: The Leading Edge, **21**, 380–387.

Voigt, W., 1910, Lehrbuch der kristallphysik (mit ausschluss der kristalloptik): BG Teubner, **34**.

Xu, S., and R. E. White, 1996, A physical model for shear-wave velocity prediction1: Geophysical Prospecting, **44**, 687–717.

Yan, J., 2002, Reservoir parameters estimation from well log and core data: a case study from the North Sea: Petroleum Geoscience, **8**, 63–69.

Yasin, I. B. E., 2012, Pressure Transient Analysis Using Generated Well Test Data from Simulation of Selected Wells in Norne Field: Master's thesis, Norwegian University of Science and Technology.

Zhang, J., 2011, Pore pressure prediction from well logs: Methods, modifications, and new approaches: Earth-Science Reviews, **108**, 50–63.

APPENDIX

A– MODELING THE EFFECTIVE ROCK ELASTIC PROPERTIES

In practice, knowing the volumetric fraction and the properties of each rock constituent is reasonable to evaluate the effective response of an specific porous medium. The concept of elastic boundaries is related to the quantitative analysis of properties of different material mixtures, describing domains to be satisfied by possible combinations of minerals and fluids. The simplest models to establish the limits of rock properties are those of Voigt (1910) and Reuss (1929), described by equations

$$E_V = \sum_{i=1}^{n} E_i f_i, \tag{A–1}$$

and

$$\frac{1}{E_R} = \sum_{i=1}^{n} \frac{f_i}{E_i}, \tag{A–2}$$

where f_i and E_i are, respectively, the volumetric fraction and the elastic property (e. g., bulk modulus) of the i-*th* constituent. Using the equation (A–1), for example, the density of fluid in the formation is estimated, taking into account an uniform mass distribution. Considering that in the fluid phase the stresses are uniformly distributed, the equation (A–2) can be used to calculate the elastic modulus of fluid.

In terms of elastic moduli, the relation of Voigt (1910) represents the maximum stiffness (isostrain condition), while the maximum compliance is indicated by the relation of Reuss (1929) (condition of isostress). To estimate a specific elastic parameter, such as the matrix bulk modulus, one can also use a simple arithmetic mean of these limits, known as Hill (1963) mean.

Another possible window of elastic moduli of a mixture of two materials is described by the expressions

$$K^{HS\pm} = K_1 + \frac{f_2}{(K_2 - K_1)^{-1} + f_1(K_1 + \frac{4}{3}\mu_1)^{-1}}, \tag{A–3}$$

and

$$\mu^{HS\pm} = \mu_1 + \frac{f_2}{(\mu_2 - \mu_1)^{-1} + 2f_1(K_1 + 2\mu_1)/[5\mu_1(K_1 + \frac{4}{3}\mu_1)]}, \tag{A–4}$$

where (K_1, μ_1) and (K_2, μ_2) are the modulus pairs of each component, and f_1 and f_2 their respective volumetric fractions. These are the bounds of Hashin-Shtrikman (Hashin and Shtrikman, 1963), which are very useful for evaluating the behavior of isotropic elastic media and has a narrower window than the Voigt-Reuss bounds. Geometrically interpreted as an arrange of spheres surrounded by a shell of different constitution, the upper bound (HS^+) is defined when the stiffest material termed as 1 forms the shell, whereas the lower bound (HS^-) is the opposite case (softest shell termed as 1 and stiffest core termed as 2).

B– GASSMANN FLUID SUBSTITUTION THEORY

From the acoustic velocities (V_p and V_s) and the bulk density (ρ_b) it is defined the volumetric shear modulus (μ) and bulk modulus (K), which are described by equations

$$\mu = \rho_b V_s^2, \tag{B–1}$$

and

$$K = \rho_b \left(V_p^2 - \frac{4}{3} V_s^2 \right), \tag{B–2}$$

where the first one quantifies the resistance of a material to tangential stress (changes of shape) and the second the resistance to compression (change of volume), both expressed in units of pressure (usually in GPa).

In order to evaluate the effect of fluid properties on acoustic velocities in saturated porous rocks we use the model proposed by Gassmann (1951). The Gassmann model is based on following assumptions: 1) the rock presents predominant homogeneity and isotropy; 2) porosity is effective (fully connected pores); 3) the fluids that fill the pores are poorly viscous; 4) the system is closed; 5) there is no chemical interaction between the rock skeleton and the fluids; and 6) there is no relative movement between the constituents of the rock in relation to the movement of the formation.

Such assumptions imply in the limitation of the Gassmann model for low frequency regime, which was later improved by Biot (1956) that considered the anomalous effects resulting from the propagation of waves at high frequencies. For both cases, Gassmann or Biot, the notion of dry rock is indispensable, corresponding to the hypothetical condition that the fluids contained in the pores of the rock skeleton are drained. Gassmann deduced a general relationship between the dry rock and saturated rock moduli, in the most common form expressed by

$$\frac{K_{sat}}{K_{min} - K_{sat}} = \frac{K_{dry}}{K_{min} - K_{dry}} + \frac{K_{fl}}{\phi(K_{min} - K_{fl})}, \tag{B–3}$$

where the subscripts sat, dry, min and fl indicate the moduli of saturated rock, dry rock, mineral matrix and fluid, respectively.

Starting from the velocity and density measurements in a given initial condition, denoted by the index (1), the following recipe is adopted for the purpose of determining velocities after fluid change:

1. The elastic moduli are extracted from the velocities of the initial condition:

$$K_{sat}^{(1)} = \rho_b^{(1)} \left(V_p^{(1)2} - \frac{4}{3} V_s^{(1)2} \right) \quad \text{and} \quad \mu_{sat}^{(1)} = \rho_b^{(1)} V_s^2;$$

2. Using Gassmann's relation the new bulk modulus is calculated:

$$K_{sat}^{(2)} = \frac{x}{(1+x)} K_{min}$$

$$x \equiv \frac{K_{sat}^{(1)}}{K_{min} - K_{sat}^{(1)}} - \frac{K_{fl}^{(1)}}{\phi(K_{min} - K_{fl}^{(1)})} + \frac{K_{fl}^{(2)}}{\phi(K_{min} - K_{fl}^{(2)})};$$

3. The shear modulus does not alter: $\mu_{sat}^{(2)} = \mu_{sat}^{(1)}$;

4. The new density is calculated: $\rho_b^{(2)} = \rho_b^{(1)} + \phi(\rho_{fl}^{(2)} - \rho_{fl}^{(1)})$;

5. Finally, we obtain the velocities in the condition denoted by the index (2):

$$V_p^{(2)} = \sqrt{\frac{K_{sat}^{(2)} + \frac{4}{3}\mu_{sat}^{(2)}}{\rho_b^{(2)}}} \quad \text{and} \quad V_s^{(2)} = \sqrt{\frac{\mu_{sat}^{(2)}}{\rho_b^{(2)}}}.$$